NASA Technical Memorandum 86277

Langley Mach 4 Scramjet Test Facility

Earl H. Andrews, Jr., Marvin G. Torrence,
Griffin Y. Anderson, G. Burton Northam,
and Ernest A. Mackley

FEBRUARY 1985

NASA

NASA Technical Memorandum 86277

Langley Mach 4 Scramjet Test Facility

Earl H. Andrews, Jr., Marvin G. Torrence,
Griffin Y. Anderson, G. Burton Northam,
and Ernest A. Mackley
Langley Research Center
Hampton, Virginia

National Aeronautics
and Space Administration

Scientific and Technical Information Branch

1985

Summary

An engine test facility has been assembled to allow tests of hydrogen-burning supersonic combustion ramjet (scramjet) engine models at simulated Mach 4 flight conditions. A three-dimensional nozzle having a nominal 13-in-square exit provides a free-jet wind-tunnel flow. Flight enthalpy is duplicated by burning hydrogen in air with oxygen replenishment to yield vitiated air containing an oxygen volumetric content of 21 percent. An air ejector enables the facility to exhaust to the atmosphere and to simulate a Mach 4 flight dynamic pressure range from 500 to 1900 psfa (altitude from 86 000 to 57 000 ft, respectively).

The facility is described and calibration test results are discussed. Some facility-engine interactions experienced in initial engine tests are briefly described. Minor hardware modifications and operational procedure changes that alleviated these interactions are discussed.

Introduction

The specific impulse I_{sp} as a function of Mach number is shown in figure 1 for several air-breathing propulsion options compared with values typical for rocket propulsion. With hydrocarbon fuels, the turbojet I_{sp} is superior over a flight speed range from take-off to a Mach number of about 3.5. From Mach 3.5 to Mach 6, the I_{sp} of the ramjet is higher. Above Mach 6, the scramjet is more efficient. The I_{sp} of these propulsion systems is increased by nearly a factor of 3, if hydrogen is burned rather than a hydrocarbon fuel.

To explore the advantages of a hydrogen-burning scramjet, a research program to develop technology for a hydrogen-burning airframe-integrated scramjet propulsion system is under way at NASA Langley Research Center (refs. 1 to 5). As part of this program a number of experimental investigations (refs. 6 to 16) and analytical investigations (refs. 17 to 25) directed toward establishing a viable concept for a scramjet propulsion system have been conducted at Langley. The proposed concept is composed of fixed-geometry modules installed together on the underside of the vehicle as shown in figure 2. This airframe-integrated engine concept takes advantage of the vehicle forebody for engine inlet precompression and the vehicle aft undersurface for continued engine nozzle expansion, as depicted in figure 2. Such a propulsion system would operate within the scramjet air-breathing corridor of which a portion is indicated in figure 3. This concept would operate with mixed subsonic-supersonic combustion over the low flight Mach number range from 3.5 to 6 and in a supersonic combustion mode for the flight Mach numbers above 6 (ref. 5).

An advantage of the modular concept is that a single module, such as that shown in figure 2(a), can be developed experimentally in reasonably sized ground test facilities that simulate the flow just ahead of the engine inlet (fig. 2(b)). Specific facility nozzle exit Mach numbers, as superimposed on the abscissa of figure 3, are required to represent the flow at the specific flight Mach numbers behind the indicated cone half-angles that are representative of vehicle forebody precompression at specific angles of attack (ref. 26). Tests simulating Mach 7 flight would allow investigations of engine fuel burning in a supersonic combustion mode. Likewise, tests simulating Mach 4 flight conditions would allow investigations of engine fuel burning in a mixed subsonic-supersonic combustion mode.

Two facilities have been assembled at NASA Langley Research Center which permit inexpensive, highly productive, combustion and engine research tests to be conducted on small-scale, gaseous-fuel-burning, scramjet models. One is an electric-arc-heated facility (refs. 27 and 28) which has the capability, with 11-in-square exit nozzles installed, as represented by the vertical bars in figure 3; scramjet engine tests have been conducted in this facility at the simulated Mach 7 flight conditions as reported in references 29 and 30. The second facility has a hydrogen-burning, vitiated-air (contains water as a product of combustion) heater with oxygen replenishment. Attachment of a Mach 3.5 contoured nozzle with a 13-in-square exit to the heater yielded a free-jet tunnel flow simulating Mach 4 flight conditions for subscale engine tests. This capability is also shown by a vertical bar in figure 3; the facility is designated the Langley Mach 4 Scramjet Test Facility (Mach 4 STF).

The potential of these facilities to simulate a wide range of test conditions is represented by the hatched areas of figure 3. The range of test capabilities of the arc heater has been demonstrated (refs. 31 and 32). The low-altitude limits of the arc heater operational envelope are dictated by the arc power available for total temperature simulations and the pressure rating of the apparatus. The high-altitude limits are dictated by the capability of the vacuum system and operation of the arc at the lower airflow rates. The potential of the Mach 4 STF is presently limited to altitudes above 57 000 ft (at Mach 4) by a low pressure rating of the vitiated-air heater duct and to altitudes below 86 000 ft by the capability of an air ejector which exhausts to the atmosphere. Proposed pressure upgrade of the heater and acquisition of a vacuum sphere exhaust system, along with additional Mach number nozzles, will allow the full potential to be realized.

The purpose of this report is to describe the Langley Mach 4 Scramjet Test Facility and to present the results of calibration tests (at nominal values of total pressure of 92 psia and total temperature of 520°R and 1630°R). Although this report addresses the facility as a Mach 4

engine test facility, the heater lends itself to other test applications, such as large-scale direct-connect combustor tests, structural component tests, and aerodynamic tests, by interchanging the hardware attached to the heater.

Symbols

A	area, in^2
d	effective exit diameter of Mach 3.5 nozzle, 14.967 in.
FOO	fuel-to-oxidizer mass flow ratio
H	nozzle exit height, 13.264 in.
I	defined by equation (2)
I_{sp}	specific impulse, (lb thrust)/(lb fuel/sec)
L	nozzle length, 50.854 in.
M	Mach number
mf	mass fraction
p	pressure, psi
q	dynamic pressure, psfa
r	radius, in.
T	temperature, °R
u	velocity, ft/sec
W	nozzle exit width, 13.264 in.
x_D	longitudinal coordinate downstream of diffuser catch-cone entrance, in.
x_N	longitudinal coordinate downstream of nozzle throat, in.
y	vertical coordinate, in.
z	lateral coordinate, in.
δ	boundary-layer thickness, in.
δ^*	boundary-layer displacement thickness, in.
θ	cone half-angle that represents sum of vehicle surface angle and angle of attack, deg
ρ	density, lb/ft^3
ϕ	fuel equivalence ratio (1.0 for stoichiometric burning)
$\dot{\omega}$	weight flow rate, lb/sec

Subscripts:

A, B, C	engine fuel injection systems
amb	ambient
avg	average
brn	burner, or heater
cab	test cabin
ej	ejector
el	elbow
FOO	based on condition that all H_2 burned stoichiometrically
H_2	hydrogen gas
H_2O	water
ign	ignitor
inj	injected
noz	nozzle exit plane
O_2	oxygen gas
s	tunnel gas flow (fig. 14)
set	hand regulator set pressure
SiH_4	silane gas
t	total or stagnation conditions
$t, 2$	pitot pressure
th	throat
$\dot{\omega}$	based on weight flow rate, $p_{t,\mathrm{brn}}$, and A_{th}
∞	free-stream conditions

Abbreviations:

DAU	data acquisition unit
ESP	electronically scanned pressure
I.D.	inside diameter
O.D.	outside diameter
STF	Scramjet Test Facility

Apparatus and Procedure

General Characteristics

The facility has a hydrogen-burning vitiated-air heater with oxygen replenishment that enables mixing and combustion research to be conducted at simulated flight conditions. Attachment of different hardware to the heater permits the facility to be used in a variety of ways to develop technology for a viable scramjet propulsion system. Installation of appropriate hardware (nozzle, combustor duct, and connections to the exhaust duct) would allow the heater to supply the proper flow

for direct-connect combustor component tests. A supersonic expansion nozzle, attached to the heater and protruding into a test cabin to produce a free-jet flow, along with the required downstream exhaust ducting, permits inlet component tests and fuel-burning engine tests to be performed.

Figures 4 and 5 show the appropriate hardware configured for a free-jet-flow tunnel to meet the requirements for fuel-burning scramjet model tests. The vitiated-air heater and the Mach 3.5 free-jet nozzle (fig. 5) produce the conditions that simulate the flow behind the bow shock of a 12° half-angle conical body at Mach 4. A total temperature $T_{t,\infty}$ of 1630°R and various tunnel total pressures produce the conditions represented by the vertical bar at $M_\infty = 4.0$ in figure 3. Total temperatures other than 1630°R with the Mach 3.5 nozzle, of course, represent different flight Mach numbers for conical bodies other than a 12° half-angle cone.

The operation map presented in figure 6 shows the facility operating characteristics and the flight conditions simulated. The sketch at the top of figure 6 indicates free-stream conditions, conditions behind the vehicle bow shock and ahead of the engine inlet that are simulated by tunnel flow, and the vehicle attitude. Curves in figure 6 that decrease with increased total pressure are lines of constant Mach number and total temperature for a given cone half-angle, and the curves that increase with pressure are lines of constant dynamic pressure. The solid line represents the characteristics of the tunnel configuration in figure 4, with the Mach 3.5 nozzle. The circles indicate calibration test points. This configuration (fig. 4) was designed for free-jet tests of hydrogen-burning scramjet models at simulated Mach 4 flight conditions and is designated the Langley Mach 4 Scramjet Test Facility (Mach 4 STF).

General Description

The Mach 4 STF test gas heater, or burner, is supplied with air, hydrogen, and oxygen from high-pressure gas storage. The hydrogen and oxygen flow rates are controlled so that the resulting combustion product mixture contains approximately 21 percent free oxygen by volume to simulate the oxygen content of air. The remaining test gas is a mixture of nitrogen and water vapor; the higher the stagnation temperature for higher simulated flight speed, the greater the hydrogen flow rate required for combustion and thus the larger the water vapor content in the test gas. Mach 4 flight simulation results in a nominal test gas composition of 8 percent water, 71 percent nitrogen, and 21 percent oxygen by volume. For convenience of facility operation, two parameters are used to describe test gas composition: the fuel-to-oxidizer mass flow ratio,

$$\mathrm{FOO} = \frac{\dot{\omega}_{H_2}}{\dot{\omega}_{air} + \dot{\omega}_{O_2}} \tag{1}$$

and the ratio of the oxygen added to the oxygen necessary to make the test gas contain the same free oxygen content as air,

$$I = \frac{\dot{\omega}_{O_2}}{12.14\dot{\omega}_{H_2}} \tag{2}$$

Note that a value of $I = 1.0$ indicates a test gas with the same oxygen content as air. Also, since the burner is always operated fuel lean (excess oxygen for combustion) and burner combustion is essentially complete, the stagnation temperature of the test gas is controlled by FOO.

The test gas from the burner is expanded through a converging-diverging nozzle to a Mach number of 3.5. This supersonic stream exhausts as a free jet into a test cabin that houses the scramjet engine. The test gas passes through and around the engine into an exhaust-duct system connected to an annular air ejector that exhausts to the atmosphere. As shown in figure 4, the test apparatus is located within a test cell that has an ambient air intake tower at the upstream end and an exhaust tower at the downstream end. The tunnel and ejector flow are directed into the entrance duct of the exhaust tower to form an ejector which induces a flow of outside air into the intake tower and through the test cell. This forced ventilation is intended to remove any hydrogen leakage which might otherwise accumulate and create an explosion hazard. Important features of the facility represented in figure 4 are described in more detail in the following sections.

Test Cell

An overall exterior view of the test cell complex is shown in figure 7. The complex contains two test cells, one of which contains the Mach 4 STF. The cells are 16 × 16 × 52 ft each and were originally constructed for combustion tests of liquid-hydrocarbon-fueled ramjet engines. They are constructed of 16-in-thick reinforced concrete walls to withstand and contain any possible apparatus failure; a cross-sectional view of a cell is shown in figure 8.

Air, cooling water, and propellants are supplied to the test cell complex. The air can be supplied to only one test cell at a time; therefore, all other systems are also shared. Physical interlocks and procedures with check lists are used to ensure the proper setup for the test cell that is in use.

Support Systems

The support systems for the test facility are shown schematically in the block diagram of figure 9. All

systems are controlled from a remotely located control room shown in figure 10. Each of these systems is briefly discussed in the following paragraphs.

Air. Air is supplied to the facility from a 600-psi system that can deliver a maximum flow rate of 300 lb/sec for approximately 3 minutes before the decreased air supply pressure adversely affects the tunnel controls. The air enters the tunnel circuit at two locations: (1) the upstream end of the test cell through a 16-in-diameter duct to the vitiated-air heater and (2) a downstream location through two 8-in-diameter lines to the air ejector.

Airflow to the heater is regulated from about 8 lb/sec for a continuous air purge to 57 lb/sec for maximum flow to the test apparatus. The airflow rate passing into the heater is determined by measuring the pressure drop across a baffle plate that was calibrated with an ASME sonic metering nozzle that is discussed in a subsequent section. The air-ejector flow rate requirement is constant at 175 lb/sec.

Cooling water. A high-pressure closed-loop cooling-water system is used to cool the heater. This system has the capability of delivering 450 gal/min at 550 psig.

Two additional water systems are also available for cooling instrumentation or for quenching the hot exhaust flow. One is a continuous water supply at about 60 psig and the other is a 500-gallon tank supply at 550 psia that can supply 50 gal/min with the present piping.

Gaseous propellants. The hydrogen, oxygen, and purge nitrogen are supplied from tube trailers visible in figure 7. The capacity of each hydrogen and oxygen tube trailer is 60 000 standard cubic feet (scf) at 2400 psia and each system can have two trailers connected for a total of 120 000 scf. The nitrogen trailer has a capacity of 47 000 scf at 2400 psia.

Pretest operations involve purging the hydrogen and oxygen piping with nitrogen, starting the continuous airflow through the tunnel, and pressurizing the systems with hydrogen and oxygen. All the piping is again purged with nitrogen during facility shutdown operations.

Hydrogen is supplied to the vitiated-air heater and also to the test model through separate remotely controlled systems. Six individually controlled and regulated systems are used to distribute the hydrogen fuel to the engine; these systems are visible in figures 5(a) and 5(b). The hydrogen flows are measured by sharp edge orifice plates (one each for the heater and engine supply), and the oxygen flow is measured with a venturi (for safety considerations). The model fuel flow is also computed for each of the six individually controlled systems with the assumption that the fuel injectors are choked and the individual flows are measured by individual line turbine flow meters to ensure accurate flow measurements at low fuel flows when the injector orifices may not be choked. For a typical engine test in the Mach 4 STF at $M_\infty = 4.0$ and $q_\infty = 1000$ psf ($p_{t,\mathrm{brn}} = 92.4$ psia and $T_{t,\mathrm{brn}} = 1630°\mathrm{R}$) the mass flow rates to the heater are 28.0 lb/sec of air, 2.35 lb/sec of oxygen, and 0.19 lb/sec of hydrogen, and the engine model hydrogen flow rate is 0 to about 0.15 lb/sec.

Hydrogen and oxygen are supplied from a separate source (220 scf at 2400 psi) to a hydrogen-oxygen torch ignitor in the vitiated-air heater. A mixture of 20 percent by volume silane (SiH_4) and hydrogen is supplied from two cylinders (220 scf at 2400 psi) to the test model to enhance ignition of the engine fuel. Silane is pyrophoric with air at atmospheric conditions and has proved to be highly successful as an ignition aid (ref. 33).

Mixer and Heater Assembly

The relative position of the mixer and heater assembly is shown in figures 4 and 5. The schematic in figure 11(a) shows some of the major details of this assembly. The design relies heavily upon the knowledge and experience gained in the design and operation of the heater in the adjacent test cell (see refs. 34 and 35). The present concept differs slightly from the heater in references 34 and 35 in that the air and oxygen are premixed in the mixer section between the oxygen and hydrogen baffle plates; thus the hydrogen is injected into oxygen-rich air. Both baffle plates have 2 rings of orifices, 10 orifices in the inner ring and 20 in the outer ring, through which injector tubes pass. Ignition of the heater propellants is provided by a hydrogen-oxygen torch ignitor that is installed as shown in figure 11. Previous designs introduced the air, hydrogen, and oxygen in proximity to one another in the heater, as discussed in references 34 and 35. Premixing the air and oxygen results in better mixing and combustion in the heater and thus allows the length-to-diameter ratio of the heater duct to be smaller than in previous designs. The design of the passages through the oxygen and hydrogen baffle plates (details presented in fig. 11(b) for the hydrogen injectors) was such that the air velocity was about $M = 0.9$ and the air-oxygen mixture velocity was about $M = 0.7$ through the respective baffle plates. Flow passages around the hydrogen injectors were modified as shown in figure 11(b) for some tests to increase the periphery flow to $M = 0.95$. Oxygen and hydrogen were injected through orifices at about $M = 0.7$. Walls of the heater duct are water jacketed (450 gal/min water flow) as shown in figure 11(a). The existing heater duct is limited to internal operating conditions of 175 psia and 2250°R.

Tunnel System

The tunnel is a free-jet design, as shown in the schematic of figure 4. The distance from the nozzle exit to the diffuser catch cone (free-jet length) was selected on the basis of the results of reference 36; this length is about 1.5 times the equivalent diameter of the square nozzle exit. A straight-duct supersonic diffuser 8 to 10 diameters long is recommended by reference 36 and others, an air-ejector mixer duct 10 or more diameters long is recommended by reference 37, and a subsonic diffuser with an expansion half-angle of 2.5° is recommended in reference 38. However, since the facility is contained within the existing 52-ft-long test cell, compromises in the supersonic-diffuser and mixer duct lengths and the subsonic-diffuser duct expansion angle were required and a turning duct was necessitated. Details of the various components of the tunnel system with these compromises are discussed in the following sections.

Nozzles. The uncooled contoured square nozzle (fig. 12(a)) was designed on the basis of the streamline-tracing concept of references 39 and 40. The throat is 4.976 in. square (24.81 in^2), and the flow exit is nominally 13 in. square (actual geometric nozzle exit dimensions are 13.264 in. to account for boundary layers). At a total temperature of 1630°R the nozzle-exit Mach number is 3.50. The nozzle entrance, which protrudes into the heater duct, makes a transition from a circular to a square cross section. The throat section was constructed with a large mass of stainless steel for heat sink, and the downstream expansion section of the nozzle was constructed of 0.183-in-thick carbon steel with external stiffening webs. The nozzle sidewalls and bottom wall were extended at the exit to ensure that shocks, generated when the ratio of cabin to nozzle-exit static pressure became equal to or greater than 2.0, would not enter the internal flow region of the engine model.

Two ASME sonic metering nozzles (figs. 12(b) and 12(c)) were used in the heater checkout and calibration tests. One nozzle had a throat area of 14.07 in^2 and was used to determine the differential pressure across the oxygen baffle to measure the air mass flow. The second nozzle had a throat area of 24.81 in^2 and was used in the diagnostic tests of the heater at operating temperatures up to 2250°R. These test results were used to generate an empirical equation for calculating the heater total temperature as a function of the heater stagnation pressure and the heater flow rates of air, hydrogen, and oxygen.

Test cabin. The test cabin (fig. 13(a)) is 30 in. wide, 42 in. high, and 96 in. long and was structurally designed for a maximum internal pressure of 35 psia which is sufficient to allow a normal shock to pass through the system during tunnel flow starting. A 9-in-diameter viewing port in each sidewall is located so that the cowl region of the engine model is visible. A 6-in-diameter viewing port in the bottom wall of the test cabin allows motion picture and television monitoring of this same region of the model.

Both sidewalls of the test cabin are easily removable (see figs. 5(a) and 13(a)) for unrestricted access to an installed model. Each sidewall is retained by 10 fuse bolts (see fig. 13(b)) that are designed to fail at a cabin internal pressure of 25 psia. Movement of only one sidewall is sufficient to relieve the overpressure. The shock-absorption system that can be seen in figure 13(a) is used to absorb the impact of the sidewalls during a cabin overpressure and to retain the sidewalls. The absorption mechanism employs fragmenting tubes (ref. 41) that are depicted in figure 13(c).

Supersonic diffuser. The supersonic diffuser (figs. 4 and 14) consists of a catch cone with a 24-in. entrance diameter and a 4.18° half-angle and of a straight duct with a 19-in. internal diameter and a length of 5.26 diameters. With the employment of an ejector, this length appeared to be sufficient. The aft 28 in. of the supersonic diffuser is actually the internal duct wall of the annular air ejector.

Air ejector and mixer. The results of reference 36 indicated that the tunnel diffuser system exhausting to the atmosphere would not provide sufficiently low back presssure for tests with large model blockage. An air ejector and mixer, diffuser, and exhaust ducting were, therefore, designed to provide the low back pressures required for such tests. The relative positions of these sections are shown in figure 4.

The annular air ejector is shown schematically in figure 14. The present ejector was designed on the basis of reference 37. Manual movement of the ejector inner wall changes the ejector annular throat and thus the ejector Mach number. Two positions of the design yield Mach numbers of 3.72 and 4.16. The ratio of ejector exit area to diffuser exit area is nearly equal to 1.0, and the nominal operational ratio of ejector mass flow to diffuser mass flow is about 6.0. Air is supplied to the tunnel and the ejector from the same source, but the mass flows are controlled separately. During a test, the tunnel and ejector airflows are stabilized prior to ignition of the heater flow.

The tunnel and ejector flows are mixed in a constant-area duct (25.25-in. I.D.) downstream of the ejector exit prior to exhausting to the atmosphere. This mixing duct has a length of 6.3 diameters.

Subsonic diffuser and exhaust. The subsonic

diffuser, located downstream of the mixer duct (fig. 14), consists of a short length of duct with a 3.8° half-angle expansion, a turning duct with internal vanes, and a short section of expanding duct with a 5° half-angle. Exhaust flow from this expanding duct passes to the atmosphere through the top of the test cell as shown in figures 4 and 8.

Test cell ventilation. To ensure that air is always flowing through the test cell before, during, and after each test, a low-pressure air ejector was installed in the test cell ceiling exhaust tower. This ejector, designed on the basis of results of reference 42, consists of a 6-ft-long duct 6-ft in diameter positioned 5 ft above the turning duct exit and protruding into the test cell exhaust tower. During tunnel pretest setup with the propellant systems pressurized into the test cell, a low flow rate of tunnel air is maintained. This tunnel air exhausts into the low-pressure ejector, entrains the test cell air, and thus ensures, for safety purposes, ventilation of the test cell.

Instrumentation and Data Systems

The facility was heavily instrumented during calibration tests and during initial engine model tests to determine the characteristics of the vitiated-air heater, the tunnel nozzle-exit flow, and the tunnel exhaust-duct flow. Locations of the instrumentation are shown schematically in figure 11(a) for the mixer and heater section and the propellant supply lines, and in figure 15 for the facility sections downstream of the heater.

Nozzle-exit rakes. Photographs and details of the various nozzle-exit rakes are shown in figure 16. A combination pitot-pressure and total-temperature survey rake, shown in figure 16(a), was installed at the exit plane of the Mach 3.5 nozzle. Details of the rake and the pitot and temperature probes are shown schematically in figure 16(b). A static-pressure rake, shown in figure 16(c), was also installed at the nozzle-exit plane. Details of the rake and probes (design based on ref. 43) are shown schematically in figure 16(d). Both rakes were mounted at identical locations in the nozzle-exit plane: on the vertical centerline and at horizontal positions z/H of 0.20, 0.35, 0.50, 0.65, and 0.80. The pitot-pressure and static-pressure rakes did not have identical probe spacing; therefore, data interpolation was necessary during data analysis. An eight-probe pitot-pressure rake, shown in the photograph of figure 16(e) and schematically in figure 16(f), was used to estimate the characteristics of the tunnel nozzle top wall boundary layer that would be ingested by engine models aligned with the nozzle top wall. This rake was mounted in three lateral locations on the nozzle top wall at the nozzle exit: y/W = 0.20, 0.35, and 0.50. At $y/W = 0.50$, a 1/8-in. shim was installed under the mounting base and a repeat of run conditions resulted in a 16-point survey. A sketch depicting probe locations during the calibration tests is shown in figure 16(g).

Data acquisition system. A schematic of the data acquisition system (DAS) for the Mach 4 STF is presented in figure 17(a). The main computer of the system, shown in the photograph of figure 17(b), is a multiprogrammable, 32-bit, general purpose digital computer with parallel 500 000 word paged memory. The DAS is designed for high-speed data acquisition and data analysis in a real-time environment. The system includes a console terminal, two disk drives (a 24 and a 48 megabyte size), a card reader, two 800 bits/in. tape drives, and a line printer. A graphics terminal was attached to the main computer over an RS-232 interface that permitted desired data to be plotted at a rate of 2400 bits/sec. A series of electronic amplifiers allowed up to 192 analog signals to be digitized. An electronically scanned pressure (ESP) measurement system (ref. 44) was attached and controlled over a standard IEEE-488 interface. The ESP is used for some of the facility duct pressure measurements, but its main purpose is to provide model pressure measurements up to 75 psia. Model thrust and drag is measured with a one-component strain-gauge force balance.

Data were recorded at a scan rate of 10 frames per second and were generally printed at a rate of 2 per second for a nominal 20-second run. The printed data are in engineering units, ratios, and/or calculations using raw data; printing starts within 1 second after the end of the test. Data are immediately plotted on the graphics terminal from which a standard set of plots is obtained on a hard copier for on-site preliminary run analysis. Once selected data are stored, the data can be recovered for additional analysis either on site or by remote computer terminals interfaced with the computer.

Procedures

The test sequence used for engine tests in the Mach 4 STF is depicted in figure 18. The pressures required to obtain the correct airflow rates to the ejector and heater, the oxygen and hydrogen flow rates to the mixer and heater, and the hydrogen flow rate to the engine are determined and preset. Duration of the test is controlled by the selected time on a run timer. Time sequences for the various engine fuel injectors are input into the automatic controller (activated by the run timer) which causes the engine fuel injector valves to open and close at selected times during the test. Once all pressure values are set, the ejector and heater

airflows are initiated, the heater ignitor is activated, and, if ignition is detected, the heater hydrogen is introduced. Combustion of the hydrogen to yield the desired facility flow total temperature causes the preset nonburning heater pressure to increase to the desired steady-state heater pressure. The heater total pressure and temperature values are digitally displayed, and once these indicate steady-state conditions, the automatic timer is initiated which starts the heater oxygen flow and sequence of events shown in figure 18 (typically 20-sec duration). After a normal run, all systems are in a dormant state but with a low tunnel airflow (8 lb/sec) for continuous tunnel purge. Within the next 5 to 10 minutes, the data are printed and stored, a standard set of data plots is obtained for desired times during the run, a preliminary run analysis is made using the printout and plots, the desired set pressures and times are changed if required, and the next run is performed. During the facility calibration tests, this procedure allowed decisions on data validity immediately after a run and the option to repeat the run if required. During engine test programs, this procedure allowed up to 12 or more runs a day.

Facility Calibration and Performance

Facility calibration and checkout were performed in three types of tests, namely, (1) unheated airflow tests with an ASME sonic metering nozzle, (2) hot flow tests with an ASME sonic metering nozzle, and (3) hot flow tests with the Mach 3.5 contoured nozzle. These tests and the results are discussed in the following sections. Facility performance during some preliminary engine tests is then discussed including some of the operational difficulties encountered and their resolution.

Sonic Nozzle Unheated Airflow Tests

Tests were performed with unheated airflow to calibrate the airflow rate as a function of pressure drop across the oxygen baffle plate (fig. 11(a)). During these tests, pressures in the heater with the unheated airflow were maintained at levels that would occur with hot flow (1630°R) at the same mass flow rates for which the facility contoured nozzle was designed. Such conditions were achieved by using an ASME sonic metering nozzle (fig. 12(b)) that was properly sized by

$$A_{\text{cold}} = A_{\text{hot}}\sqrt{\frac{T_{\text{cold}}}{T_{\text{hot}}}} \tag{3}$$

The standard mass flow rate equation for choked flow was used with the nozzle throat area, heater duct stagnation pressure, and heater duct stagnation temperature to determine the unheated air mass flow. Pressures measured in the nozzle throat ensured high nozzle efficiency.) These flow values, the measured pressure upstream of the oxygen baffle plate, and the differential pressure (Δp) across the oxygen baffle plate were used to determine an empirical equation of the air weight flow based on the baffle-plate pressure measurements:

$$\dot{\omega}_{\text{air}} = 0.59309 - 0.40103\frac{\Delta p}{p} \tag{4}$$

Sonic Nozzle Hot Flow Tests

Once the unheated airflow calibration tests were completed, a larger ASME sonic metering nozzle (fig. 12(c)) was installed for tests to examine the heater operation. The throat area (5.62-in. diameter) of this Mach 1.0 nozzle was equal to the throat area of the Mach 3.5 contoured square nozzle (fig. 12(a)). Tests were conducted with heated flow at total temperatures of 1630°R and stagnation pressures in the heater of 46.0, 69.0, 92.0, and 160 psia (Mach 4 flight dynamic pressures of 500, 750, 1000, and 1730 psfa, respectively). A few tests were performed at a total temperature of 2250°R and a total pressure of 92.4 psia (Mach 5 flight total enthalpy and dynamic pressure of 575 psfa).

Total-temperature determination. The following procedure was adopted to estimate the bulk total temperature of the facility nozzle-exit flow using the measured burner pressure, gas flows supplied to the burner, and the known nozzle throat area. The stagnation temperature in the heater for the oxygen-replenished test gas ($I = 1.0$) was determined from real-gas thermodynamic calculations using a computer program such as that used in reference 34 and is a function of the fuel-to-oxidizer mass flow ratio, FOO (see eq. (1)). For convenience, the theoretical stagnation temperature with complete combustion was correlated in a fourth order polynomial fit as a function of FOO as follows:

$$\begin{aligned} T_{t,\text{FOO}} =& (-1.3939 \times 10^9)\text{FOO}^4 \\ &+ (1.1313 \times 10^8)\text{FOO}^3 \\ &+ (-5.0144 \times 10^6)\text{FOO}^2 \\ &+ (2.2255 \times 10^5)\text{FOO} + 524.47 \end{aligned} \tag{5}$$

For a sonic throat the stagnation temperature is related to the stagnation pressure and total mass flow by the relationship

$$T_{t,\dot{\omega}} = \left[\frac{(\text{FKA})p_{t,\text{brn}}A_{\text{th}}}{\dot{\omega}_{\text{brn}}}\right]^2 \tag{6}$$

The parameter FKA which would be constant for a perfect gas is a weak function of stagnation temperature and FOO for nearly complete combustion. Again, a fourth order polynomial fit was used to specify FKA as a function of FOO alone for complete combustion:

$$\begin{aligned}\mathrm{FKA} =&(-3.5152 \times 10^4)\mathrm{FOO}^4 \\ &+ (1.1313 \times 10^3)\mathrm{FOO}^3 \\ &+ (29.242)\mathrm{FOO}^2 \\ &+ (-2.9953)\mathrm{FOO} + 0.53214 \end{aligned} \tag{7}$$

An initial estimate of $T_{t,\dot{\omega}}$ was then obtained from equation (6) with the measured values of $p_{t,\mathrm{brn}}$, A_{th}, and $\dot{\omega}_{\mathrm{brn}}$.

This estimate of $T_{t,\dot{\omega}}$, which is based on a value of FKA corresponding to complete reaction, was then used to estimate the heat loss (HL) to the water-cooled heater and heat sink nozzle walls and to iterate to a corrected value of nozzle-exit total temperature as follows:

$$\mathrm{HL}(n) \approx \frac{T_{t,\mathrm{FOO}} - T_{t,\dot{\omega}}(n)}{T_{t,\mathrm{FOO}} - T_{\mathrm{amb}}} \tag{8}$$

A correction for FKA was calculated from a power fit to theoretical results for complete reaction where

$$K(n) = 66.3\,\mathrm{FOO}^{2.07}\,\mathrm{HL}(n) \tag{9}$$

and the corrected value is

$$\mathrm{FKA}' = \mathrm{FKA}[1.0 + K(n)] \tag{10}$$

The corrected value for FKA was then substituted in equation (6). This iteration procedure was performed only five times since changes in properties are small with heat loss, with the value of $T_{t,\dot{\omega}}(n)$ on the fifth iteration taken as an estimate of the bulk gas temperature $T_{t,\mathrm{brn}}$ at the nozzle exit.

Comparison of this computed temperature with the theoretical temperature indicated a heat loss of about 11.0 percent. A total heat loss of about 10 to 11 percent was indicated to be a reasonable value in reference 34. During these tests, the measured rise in the heater duct cooling water temperature indicated a heat gain of about 6 to 8 percent of the heater fuel energy. Heat loss to the nozzle was not measured but was estimated to be about 3 to 5 percent.

Total temperature affected by air-oxygen injection velocity. Heater diagnostic tests were performed with two different velocities of the air-oxygen mixture at the heater hydrogen injectors. The two different arrangements of the hydrogen injection tubes in relation to the air-oxygen passage tubes shown in figure 11(b) yielded air-oxygen velocities corresponding to $M \approx 0.7$ and 0.95.

Data from several tests with the higher air-oxygen velocity ($M \approx 0.95$) indicated that the total temperature based on the sonic throat calculations was much less than the theoretical combustion temperature and did not parallel the theoretical curve, as shown in figure 19. Also, higher values of FOO than desired were required to ensure heater ignition, and the heater became unstable with possible "flameout" at FOO less than 0.007. The increased air-oxygen velocity was apparently too great to allow complete combustion. The tube arrangements (fig. 11(b)) were then changed to yield the present lower air-oxygen velocity ($M \approx 0.7$), and the resulting total-temperature values based on the sonic throat calculation were somewhat less but parallel to the theoretical combustion temperature curve, as shown in figure 19. The heater then operated in a stable mode at bulk temperatures down to approximately 1300°R.

Operating Parameters

Standard thermodynamic computations for combustion of hydrogen in air with oxygen replenishment (developed into a computer program and previously used, e.g., ref. 34) yield parameters such as those presented in figure 20. During the Mach 1.0 hot flow tests, the heat loss to the heater and nozzle walls was determined and the mixture ratio curve of figure 20(a) was corrected as represented by the cross-hatched band (representing accuracy). Using the corrected band to relate a desired heater temperature to the no-heat-loss temperatures, one can determine the required mass fractions of hydrogen, oxygen, and air. From these, the facility operational parameters can be determined which will produce simulated air (correct amount of oxygen) at the proper total temperature for experimental combustion investigations. Operational parameters ($p_{t,\mathrm{brn}}$, $T_{t,\mathrm{brn}}$, and total mass flow) for a nozzle throat area of 24.81 in^2 are presented in figure 21. The required tunnel total pressure necessary to simulate a particular altitude, or dynamic pressure, at $M = 4$ and 1600°R (point A in fig. 21) is used to determine the tunnel total mass flow rate and thereby indicate the burner total pressure for air only at 530°R (point B in fig. 21). From the Mach 1.0 unheated airflow tests, the upstream pressure settings were correlated with the heater total pressure and are represented in figure 22(a); point B of figure 21 is used on figure 22(a) to determine air pressure setting. The heater hydrogen and oxygen mass flows required are related to the upstream pressure settings (on the control panel gauges) and the injected pressures. These pressures are also correlated with the hot flow heater total pressure represented by point A in figure 22(b). The proper settings for desired test conditions determined from curves such as those shown in figures 21 and 22 allowed good test condition repeatability.

Nozzle Calibration

Once the heater flow calibration tests were com-

pleted and the appropriate operating parameter settings were determined for good test condition repeatability, facility nozzle flow calibration tests were performed. These tests were performed at nominal values of total pressure (92 psia) and total temperature (520°R and 1630°R) with the survey rakes described in figure 16 positioned at the exit of the basic nozzle ($x_N = 50.854$ in.) without the nozzle extension installed (fig. 12(a)) and at the positions depicted in figure 16(g).

In analyzing test data, it was noted that the nozzle wall static pressure near the exit, $x_N = 48.35$ in. ($x_N/L = 0.95$), was consistently higher than the upstream pressure at $x_N = 39.1$ in. ($x_N/L = 0.77$), as shown in figure 23. Examination of the nozzle indicated that an inner wall surface distortion that resulted from external welding of a flange to the nozzle external surface at $x_N \approx 42.0$ in. ($x_N/L = 0.83$) was the cause of the slight flow compression. The total-pressure loss associated with this wall distortion and its impact on nozzle-exit flow uniformity is negligible.

A nozzle-exit wall pressure was calculated by assuming a one-dimensional isentropic expansion from the area and pressure at $x_N = 39.1$ in. to the exit area with Mach number determined from $p_{noz}/p_{t,brn}$. All subsequent analyses involving an exit wall pressure were made using this calculated p_{noz}. Average exit Mach numbers, based on p_{noz} and burner total pressure, were 3.55 and 3.52 for the unheated airflow and hot flow test conditions, respectively.

Survey data. The results of the surveys are presented in figures 24 and 25 for the unheated airflow and hot flow conditions ($T_{t,brn}$ nominally 520°R and 1630°R), respectively. The nozzle-exit flow was uniform and symmetrical for both cold and hot conditions. Quantitatively the data compared well when the Mach number and mass flow were calculated using various combinations of the measured parameters. Results of a survey made with the pitot-pressure rake on the exit vertical centerline were consistent with horizontal survey center-point values.

Pitot-pressure data, nondimensionalized by burner total pressure, are presented in figures 24(a) and 25(a). Small deviations of nonuniformity are noted but are considered acceptable for such tunnel flow. These small nonuniformities are, however, symmetric about the nozzle centerline.

Total-temperature data, nondimensionalized by burner total temperatures (based on weight flow), are presented in figures 24(b) and 25(b). Thermocouple probe failures occurred during some of the tests because of tunnel vibration causing wire breakage or electrical shorts; failures are evident by missing data points. The high-temperature data exhibit nonuniform trends which are not readily explainable. The profile for the vertical centerline is, however, very uniform. Overall, the nozzle-exit total-temperature profiles are considered sufficiently uniform for testing scramjet engines.

The static-pressure survey data normalized by the burner total pressure are presented in figures 24(c) and 25(c). Both distributions are very uniform. The static-pressure rake contained five probes and the wall values plotted at $y/W = 0$ and 1.0 are the calculated exit wall pressure p_{noz}. For both test conditions, the free-stream survey pressures agree well with the nozzle wall pressures.

The nozzle top wall boundary layer was surveyed with the seven-probe stationary pitot-pressure rake. Measurements were made on the vertical centerline and at lateral positions of $y/W = 0.20$ and 0.35. Assuming a constant static pressure p_{noz} through the boundary layer, the local Mach number was calculated from the pitot survey data. Velocity distributions were then obtained from the Mach number and an assumed constant total temperature. From the turbulent boundary-layer velocity profiles (not shown), the thickness δ was estimated. In the unheated airflow cases, velocity profiles could be interpreted to show $\delta = 1$ in. or 0.75 in. Therefore, the data for unheated airflow were analyzed with both values. For the hot flow conditions, the thickness δ was shown to be 1 in. at all three positions. From the local Mach number, constant static pressure (p_{noz}), and total temperatures, boundary-layer mass flow distributions were determined and are shown in figures 24(d) and 25(d); distance from the wall is measured in inches and local mass flow per unit area is nondimensionalized by the free-stream value. The boundary-layer displacement thickness δ^* was then evaluated from

$$\frac{\delta^*}{\delta} = \int_0^{1.0} \left(1 - \frac{\rho u}{\rho_\infty u_\infty}\right) d\left(\frac{z}{\delta}\right) \qquad (11)$$

Integration of the plots in figure 24(d) (unheated airflow) produced a value of $\delta^* \approx 0.23$ in. for $y/H = 0.5$ and 0.35 and $\delta^* \approx 0.17$ in. at $y/H = 0.2$. These integrated values of δ^* were the same for both values of δ (1.0 and 0.75 in.). For the hot flow cases (fig. 25(d)), an average value of $\delta^* = 0.23$ in. was found for the three rake positions. This value ($\delta^* = 0.23$) was assumed to be constant in subsequent analyses involving boundary-layer mass flow deficit.

Mach number profiles are shown in figures 24(e), 24(f), 25(e), and 25(f). Where the boundary layers influence the results, nonuniformities are evident for all cases and are most prominent near the walls. The values at y/W of 0.5 and 0.95 based on $p_{t,2}/p_{t,brn}$ are therefore in error since the total pressures at these points are not equal to $p_{t,brn}$.

Mass flow rates. To assess the accuracy of the calibration data, an estimate of the nozzle-exit mass

flow was made for comparison with the metered tunnel flow. Mass flow integration was accomplished by the summation of flows through incremental areas assigned at survey points. A sketch of this integration map is shown in figure 26. The dashed-line rectangle represents the capture area of a scramjet inlet. Because of some uncertainty of the survey data, the Mach number and corresponding mass flow per unit area at the survey points were calculated from the four measured pressure parameters, $p_{t,2}/p_{t,\mathrm{brn}}$, $p_\infty/p_{t,2}$, $p_\infty/p_{t,\mathrm{brn}}$, and $p_{\mathrm{nozz}}/p_{t,2}$. All calculations were made for real gas (thermally perfect). The integration results are tabulated in table I.

In general, good agreement exists between the measured bulk flow rates and the flow rates obtained from integrations of the survey results. The average Mach number shown is simply an arithmetic average of the survey point values. Average Mach number in the calculations using survey static pressure (p_∞) for the unheated airflow conditions ($T_{t,\mathrm{brn}} = 520°\mathrm{R}$) appears to be low. The Mach number derived from pitot measurements is considered more reliable because of the sensitivity of static-pressure probes to flow misalignment.

Flow angularity. A brief study of flow angularity was conducted during unheated airflow tests using a single 25° half-angle conical probe (ref. 45). The probe tip was blunted to 0.025 in. in diameter to accept a 0.010-in-diameter pitot-pressure orifice. Four individual 0.020-in-diameter static-pressure orifices were located 0.360 in. from the cone tip. The probe was mounted and accurately aligned with the horizontal. Measurements were taken in the nozzle-exit plane ($x_N = 50.854$ in.) on the nozzle axis and 2 in. above the horizontal centerline on the vertical centerline. Yaw alignment of the probe was performed by accurately mounting the probe parallel to the nozzle walls.

The pressure measurements obtained with this probe were used along with references 46 to 48. Results indicated a nozzle-exit Mach number of 3.55 which agreed with the nozzle-exit pitot survey results. Nozzle flow angularity was shown to be less than 1° in the downward direction, which is within the mounting accuracy of the probes and model installation.

Facility-Engine Interactions

During initial research tests of a hydrogen-burning scramjet engine model, interactions between the facility and engine occurred as fuel injection into the model was increased, especially if poor engine combustion occurred. Exhaust-duct wall pressure and stationary pitot-pressure rake measurements indicated the onset of these disturbances; figure 27(a) shows the relative locations of the wall pressure measurements and rakes. The unburned engine fuel apparently ignited in the duct and generated back pressure that eventually affected the tunnel flow in the region of the engine and, at times, caused the tunnel nozzle flow to separate. Several techniques were attempted to eliminate these facility-engine interactions. A combination of high burner total pressure ($p_{t,\mathrm{brn}} \approx 160$ psia) and water sprayed into the diffuser catch cone and at the elbow turning vane leading edges was found to be most successful. This technique resulted in the undisturbed measurements of figure 27(b). During a later engine test program with improved engine fuel mixing and burning, successful tests could be performed at lower burner total pressures ($p_{t,\mathrm{brn}} \approx 92$ psia). Also, replacement of the nozzle extension shown in figure 12(a) with an extension 9 in. longer decreased the facility free-jet length and made the nozzle flow less sensitive to increases in the exhaust-duct back pressure. The success of all of the above means of resolving the facility-engine interaction is also evident in figure 27(c). Prior to the resolution of the interaction problem, the increased pressures in the exhaust system affected the engine measurements. When the engine inlet flow "unstarted," the facility nozzle flow was drastically affected. Data of a post-resolution test indicated that an engine combustor-inlet interaction, caused by combustor fuel-burning pressure rise, occurred before tunnel disturbances. Also, after the changes were made, even with the inlet unstarted and a facility flow breakdown, the facility nozzle flow was seldom affected. With the present Mach 4 STF configurations, hydrogen-burning scramjet models which block 35 percent of the tunnel flow cross section have been successfully tested (refs. 49 to 51).

Concluding Remarks

A test facility has been assembled at NASA Langley Research Center to provide the capability for various types of air-breathing propulsion research, that is, inlet tests, fuel-air mixing experiments, direct-connect combustor tests, or engine tests. Hydrogen is burned in air with oxygen replenishment to yield simulated air with the proper oxygen content for combustion tests. The present configuration downstream of the heater is a free-jet wind tunnel with a three-dimensional Mach 3.5 nozzle (nominal 13-in-square exit) for simulation of Mach 4 flight conditions at the inlet of an airframe-integrated scramjet.

The overall results of the calibration tests of the Langley Mach 4 Scramjet Test Facility indicate that the uniformity of the nozzle-exit flow is adequate for testing hydrogen-burning scramjet engine models. Nozzle-exit Mach number was determined to be nominally 3.52 for the Mach 4 hot (1630°R) flow conditions, and nozzle-exit flow angularity measured during unheated inflow tests (520°R) was less than 1° in the downward

direction. In a current research program for developing technology for a hydrogen-burning airframe-integrated scramjet, models which block as large as 35 percent of the tunnel flow cross section have been successfully tested.

Langley Research Center
National Aeronautics and Space Administration
Hampton, VA 23665
October 1, 1984

References

1. Waltrup, Paul J.; Anderson, Griffin Y.; and Stull, Frank D.: Supersonic Combustion Ramjet (Scramjet) Engine Development in the United States. *Proceedings—3rd International Symposium on Air Breathing Engines*, Dietmar K. Hennecke and Gert Winterfeld, eds., DGLR—Fachbuchreihe Bd. 6, 1976, pp. 835–861.
2. Henry, John R.; and Anderson, Griffin Y.: *Design Considerations for the Airframe-Integrated Scramjet.* NASA TM X-2895, 1973.
3. Jones, Robert A.; and Huber, Paul W.: Toward Scramjet Aircraft. *Astronaut. & Aeronaut.*, vol. 16, no. 2, Feb. 1978, pp. 38–48.
4. Jones, Robert A.; and Huber, Paul W.: Airframe-Integrated Propulsion System for Hypersonic Cruise Vehicles. *ICAS Proceedings—1978, Volume 1, Fuel Conservation, Hypersonic Vehicles, Environmental Effects, Materials and Structures, Computational Aerodynamics, Wind Tunnels, Flight Testing, Stability and Control*, J. Singer and R. Staufenbiel, eds., Sept. 1978, pp. 130–136.
5. Beach, H. Lee, Jr.: Hypersonic Propulsion. *Aeropropulsion 1979*, NASA CP-2092, 1979, pp. 387–401.
6. Trexler, Carl A.; and Souders, Sue W.: *Design and Performance at a Local Mach Number of 6 of an Inlet for an Integrated Scramjet Concept.* NASA TN D-7944, 1975.
7. Trexler, Carl A.: Inlet Performance of the Integrated Langley Scramjet Module (Mach 2.3 to 7.6). AIAA Paper No. 75-1212, Sept.-Oct. 1975.
8. Anderson, Griffin Y.: Hypersonic Propulsion. *Aeronautical Propulsion*, NASA SP-381, 1975, pp. 459–469.
9. Rogers, R. C.; and Eggers, J. M.: Supersonic Combustion of Hydrogen Injected Perpendicular to a Ducted Vitiated Airstream. AIAA Paper No. 73-1322, Nov. 1973.
10. Anderson, Griffin Y.; Eggers, James M.; Waltrup, Paul J.; and Orth, Richard C.: Investigation of Step Fuel Injectors for an Integrated Modular Scramjet Engine. *13th JANNAF Combustion Meeting*, Volume III, CPIA Publ. 281 (Contract N00017-72-C-4401), Appl. Phys. Lab., Johns Hopkins Univ., Dec. 1976, pp. 175–189.
11. Rogers, R. C.: Influence of Fuel Temperature on Supersonic Mixing and Combustion of Hydrogen. AIAA Paper 77-17, Jan. 1977.
12. Anderson, Griffin Y.; and Gooderum, Paul B.: *Exploratory Tests of Two Strut Fuel Injectors for Supersonic Combustion.* NASA TN D-7581, 1974.
13. McClinton, C. R.; and Gooderum, P. B.: Direct-Connect Test of a Hydrogen-Fueled Three-Strut Injector for an Integrated Modular Scramjet Engine. *14th JANNAF Combustion Meeting*, Volume II, T. W. Christian, ed., CPIA Publ. 292 (Contract N00017-72-C-4401), Appl. Phys. Lab., Johns Hopkins Univ., Dec. 1977, pp. 489–505.
14. Anderson, Griffin Y.; Reagon, Patricia G.; Gooderum, Paul B.; and Russin, W. Roger: *Experimental Investigation of a Swept-Strut Fuel-Injector Concept for Scramjet Application.* NASA TN D-8454, 1977.
15. Northam, G. B.; Trexler, C. A.; and Anderson, G. Y.: Characterization of a Swept-Strut Hydrogen Fuel-Injector for Scramjet Applications. *15th JANNAF Combustion Meeting*, Volume III, T. W. Christian, ed., CPIA Publ. 297 (Contract N00024-78-C-5384), Appl. Phys. Lab., Johns Hopkins Univ., Feb. 1979, pp. 393–410.
16. McClinton, Charles R.: Autoignition of Hydrogen Injected Transverse to a Supersonic Airstream. AIAA Paper 79-1239, June 1979.
17. Pan, Y. S.: *The Development of a Three-Dimensional Partially Elliptic Flow Computer Program for Combustor Research.* NASA CR-3057, 1978.
18. Pan, Y. S.; Drummond, John Philip; and McClinton, Charles R.: *Comparison of Two Computer Programs by Predicting Turbulent Mixing of Helium in a Ducted Supersonic Airstream.* NASA TP-1166, 1978.
19. Pan, Y. S.: *Evaluation of the Three-Dimensional Parabolic Flow Computer Program SHIP.* NASA TM-74094, 1978.
20. Rogers, R. C.: A Model of Transverse Fuel Injection Applied to the Computation of Supersonic Combustor Flow. AIAA Paper No. 79-0359, Jan. 1979.
21. Drummond, J. Philip: Numerical Solution for Perpendicular Sonic Hydrogen Injection Into a Ducted Supersonic Airstream. *AIAA J.*, vol. 17, no. 5, May 1979, pp. 531–533.
22. Drummond, J. Philip: Numerical Investigation of the Perpendicular Injector Flow Field in a Hydrogen Fueled Scramjet. AIAA Paper 79-1482, July 1979.
23. Drummond, J. Philip; and Weidner, Elizabeth H.: Numerical Study of a Scramjet Engine Flow Field. AIAA-81-0186, Jan. 1981.
24. Drummond, J. Philip; and Weidner, Elizabeth H.: A Numerical Study of Candidate Transverse Fuel Injector Configurations in the Langley Scramjet Engine. *17th JANNAF Combustion Meeting*, Volume I, Debra Sue Eggleston, ed., CPIA Publ. 329 (Contract N00024-78-C-5384), Appl. Phys. Lab., Johns Hopkins Univ., Nov. 1980, pp. 561–586.
25. Weidner, Elizabeth H.; and Drummond, J. Philip: A Parametric Study of Staged Fuel Injector Configurations for Scramjet Applications. AIAA-81-1468, July 1981.
26. Weidner, J. P.; Small, W. J.; and Penland, J. A.: Scramjet Integration on Hypersonic Research Airplane Concepts. *J. Aircr.*, vol. 14, no. 5, May 1977, pp. 460–466.

27. Boatright, William B.; Sabol, Alexander P.; Sebacher, Daniel I.; Pinckney, Shimer Z.; and Guy, Robert W.: Langley Facility for Tests at Mach 7 of Subscale, Hydrogen-Burning, Airframe-Integratable, Scramjet Models. AIAA Paper No. 76-11, Jan. 1976.
28. Guy, Robert W.; Torrence, Marvin G.; Sabol, Alexander P.; and Mueller, James N.: Operating Characteristics of the Langley Mach 7 Scramjet Test Facility. NASA TM-81929, 1981.
29. Guy, Robert W.; and Mackley, Ernest A.: Initial Wind Tunnel Tests at Mach 4 and 7 of a Hydrogen-Burning, Airframe-Integrated Scramjet. *Fourth International Symposium on Air Breathing Engines*, Apr. 1979, pp. 347–358. (Available as AIAA Paper 79-7045.)
30. Guy, Robert W.; Torrence, Marvin G.; Mueller, James N.; and Sabol, Alexander P.: *Initial Ground-Facility Tests at Mach 7 of a Hydrogen-Burning, Airframe-Integrated, Scramjet-Engine Model.* NASA TM-84644, 1983.
31. Thomas, Scott R.; and Guy, Robert W.: Increased Capabilities of the Langley Mach 7 Scramjet Test Facility. AIAA-82-1240, June 1982.
32. Thomas, Scott R.; and Guy, Robert W.: *Expanded Operational Capabilities of the Langley Mach 7 Scramjet Test Facility.* NASA TP-2186, 1983.
33. Beach, H. L., Jr.; Mackley, E. A.; Rogers, R. C.; and Chinitz, W.: Use of Silane in Scramjet Research. *17th JANNAF Combustion Meeting*, Volume I, Debra Sue Eggleston, ed., CPIA Publ. 329 (Contract N00024-78-C-5384), Appl. Phys. Lab., Johns Hopkins Univ., Nov. 1980, pp. 639–659.
34. Russin, William Roger: *Performance of a Hydrogen Burner To Simulate Air Entering Scramjet Combustors.* NASA TN D-7567, 1974.
35. Eggers, James M.: *Composition Surveys of Test Gas Produced by a Hydrogen-Oxygen-Air Burner.* NASA TM X-71964, 1974.
36. Andrews, E. H., Jr.; and Mackley, E. A.: Design, Tests, and Verification of a Diffuser System for a Mach 4 Scramjet Test Facility. *J. Aircr.*, vol. 16, no. 10, Oct. 1979, pp. 641–642. (Available as AIAA Paper 78-771, revised.)
37. Hasinger, Siegfried H.: *Performance Characteristics of Ejector Devices.* ARL-75-0205, U.S. Air Force, June 1975. (Available from DTIC as AD A015 040.)
38. *Handbook of Supersonic Aerodynamics, Section 17—Ducts, Nozzles and Diffusers.* NAVWEPS Rep. 1488, U.S. Navy, Jan. 1964. (Available from DTIC as AD 418 060.)
39. Evvard, John C.; and Maslen, Stephen H.: *Three-Dimensional Supersonic Nozzles and Inlets of Arbitrary Exit Cross Section.* NACA TN 2688, 1952.
40. Beckwith, Ivan E.; and Moore, John A.: *An Accurate and Rapid Method for the Design of Supersonic Nozzles.* NACA TN 3322, 1955.
41. McGehee, John R.: *Experimental Investigation of Parameters and Materials for Fragmenting-Tube Energy-Absorption Process.* NASA TN D-3268, 1966.
42. Kastner, L. J.; and Spooner, J. R.: An Investigation of the Performance and Design of the Air Ejector Employing Low-Pressure Air as the Driving Fluid. *Proc. Inst. Mech. Eng. (London)*, vol. 162, no. 2, 1950, pp. 149–159.
43. Pinckney, S. Z.: *A Short Static-Pressure Probe Design for Supersonic Flow.* NASA TN D-7978, 1975.
44. Trexler, C. A.: Instant-Replay Data System for Combustion Tests. *17th JANNAF Combustion Meeting*, Volume I, Debra Sue Eggleston, ed., CPIA Publ. 329 (Contract N00024-78-C-5384), Appl. Phys. Lab., Johns Hopkins Univ., Nov. 1980, pp. 469–479.
45. Eng. Staff, AiResearch Manufacturing Co. of California: *Hypersonic Research Engine Project—Phase II Aerothermodynamic Integration Model Development Final Technical Data Report.* Doc. No. AP-75-11133 (Contract NAS1-6666), May 19, 1975. (Available as NASA CR-132654.)
46. Ames Research Staff: *Equations, Tables, and Charts for Compressible Flow.* NACA Rep. 1135, 1953. (Supersedes NACA TN 1428.)
47. Swalley, Frank E.: *Measurement of Flow Angularity at Supersonic and Hypersonic Speeds With the Use of a Conical Probe.* NASA TN D-959, 1961.
48. Sims, Joseph L.: *Tables for Supersonic Flow Around Right Circular Cones at Zero Angle of Attack.* NASA SP-3004, 1964.
49. Andrews, E. H.; Northam, G. B.; Torrence, M. G.; and Trexler, C. A.: Mach 4 Tests of a Hydrogen-Burning Airframe-Integrated Scramjet. *18th JANNAF Combustion Meeting*, Volume IV, Debra Sue Eggleston, ed., CPIA Publ. 347 (Contract N00024-81-C-5301), Appl. Phys. Lab., Johns Hopkins Univ., Oct. 1981, pp. 87–96.
50. Andrews, Earl H.; Northam, G. Burton; Torrence, Marvin G.; Trexler, Carl A.; and Pinckney, S. Zane: *Mach 4 Wind-Tunnel Tests of a Hydrogen-Burning Airframe-Integrated Scramjet Engine.* NASA TM-85688, 1984.
51. Andrews, E. H.; Guy, R. W.; Pinckney, S. Z.; and Torrence, M. G.: Mach 4.0 Tests of a Hydrogen-Fueled Parametric Airframe-Integrated Scramjet. *1984 JANNAF Propulsion Meeting*, Volume V, Karen L. Strange, ed., CPIA Publ. 390, Vol. V (Contract N00024-83-C-5301), Appl. Phys. Lab., Johns Hopkins Univ., Feb. 1984, pp. 153–167.

TABLE I. MASS FLOW INTEGRATION RESULTS

Parameter	$p_{t,2}/p_{t,\mathrm{brn}}$		$p_\infty/p_{t,2}$		$p_\infty/p_{t,\mathrm{brn}}$		$p_{\mathrm{nos}}/p_{t,2}$	
$T_{t,\mathrm{brn}}$, °R	520	1630	520	1630	520	1630	520	1630
Measured flow rate, lb/sec	54	31	54	31	54	31	54	31
Integrated flow rate without boundary layer, lb/sec	53	31	50	30	53	31	50	30
Integrated flow rate with boundary layer, lb/sec	50	29	47	28	49	29	50	28
Average M_{nos}	3.55	3.53	3.42	3.51	3.52	3.52	3.56	3.52

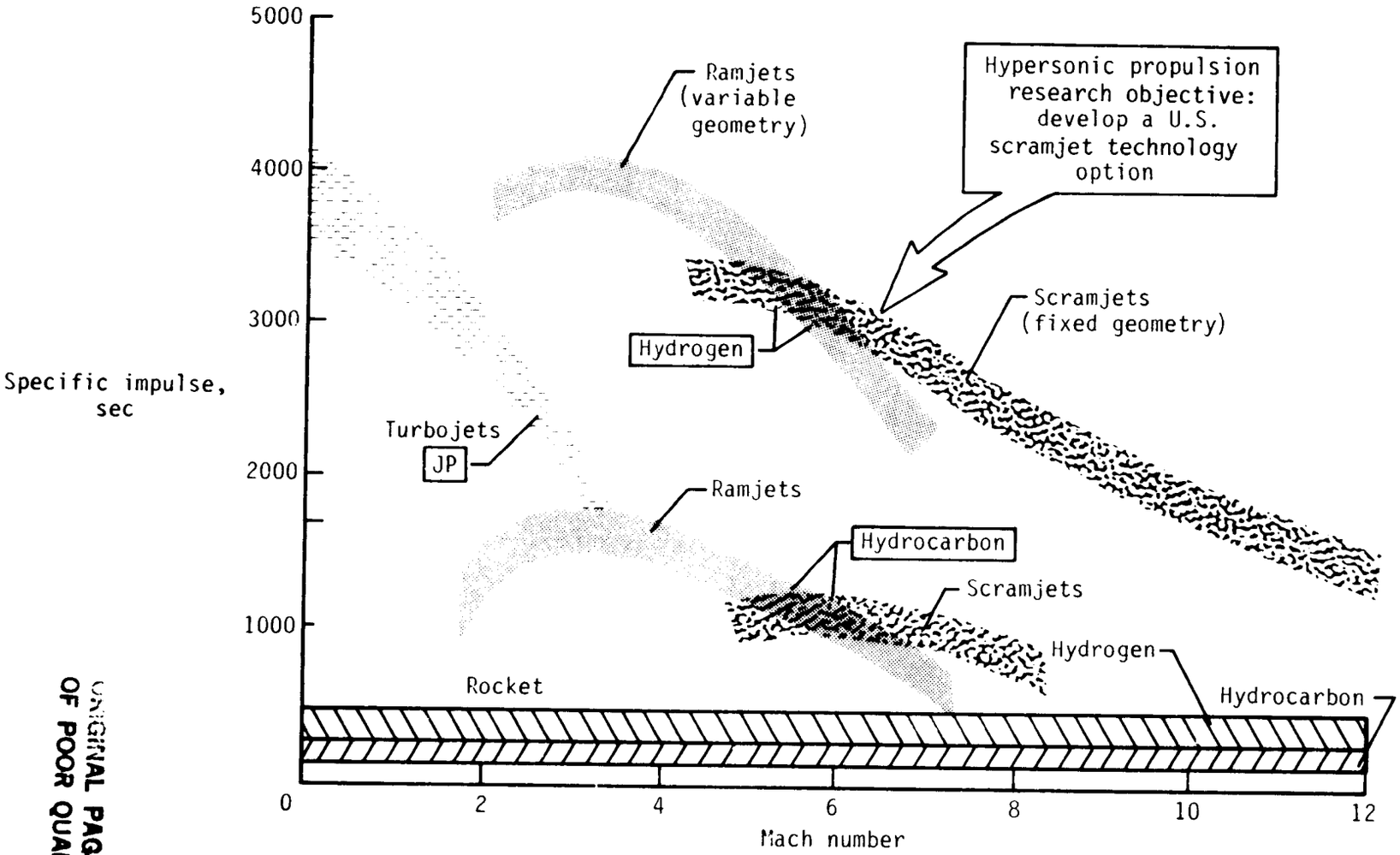

Figure 1. Propulsion system efficiencies.

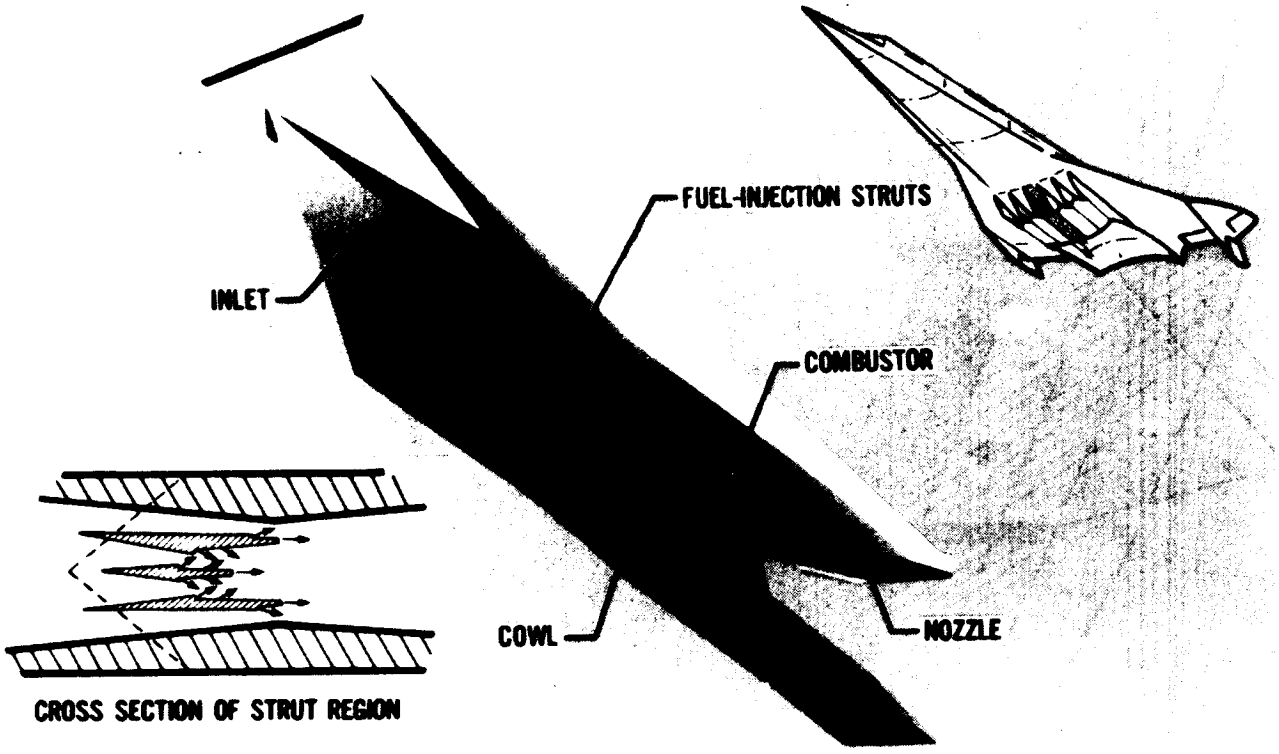

L-84-10,655

(a) Integrated concept.

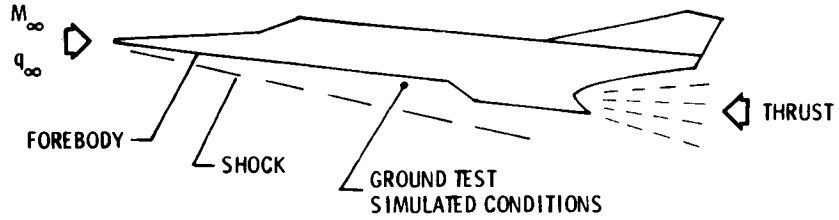

(b) Simulated conditions.

Figure 2. Airframe-integrated scramjet.

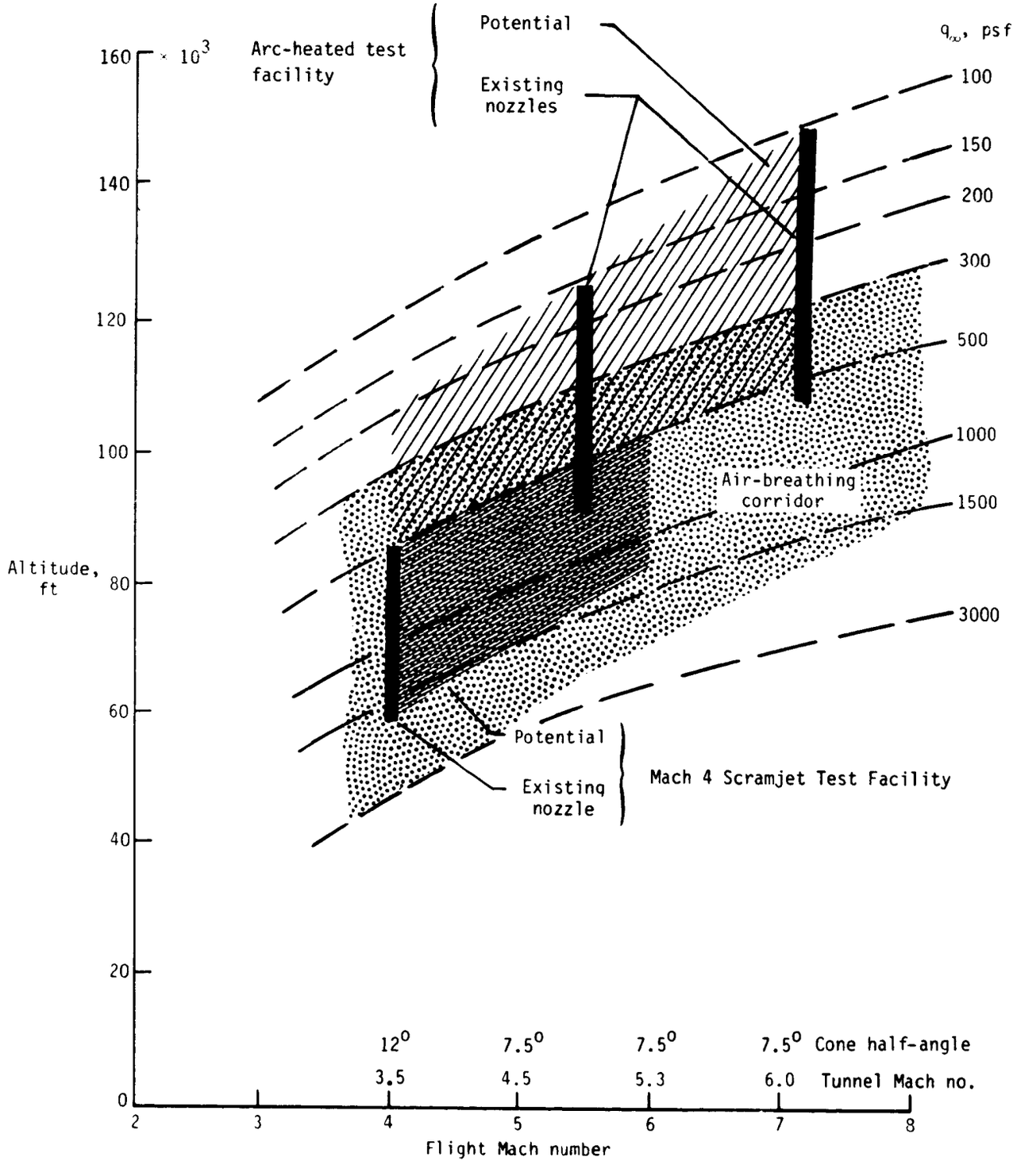

Figure 3. Typical dual-mode scramjet operation flight envelope.

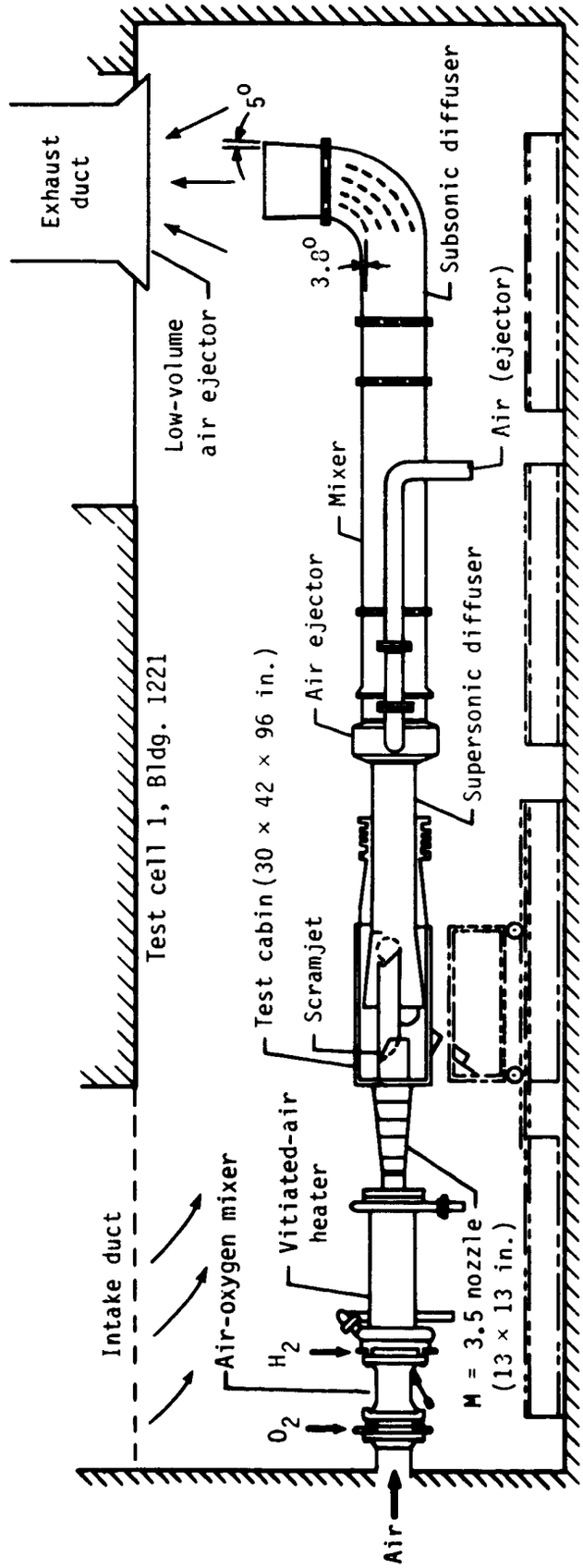

Figure 4. Schematic of Langley Mach 4 Scramjet Test Facility.

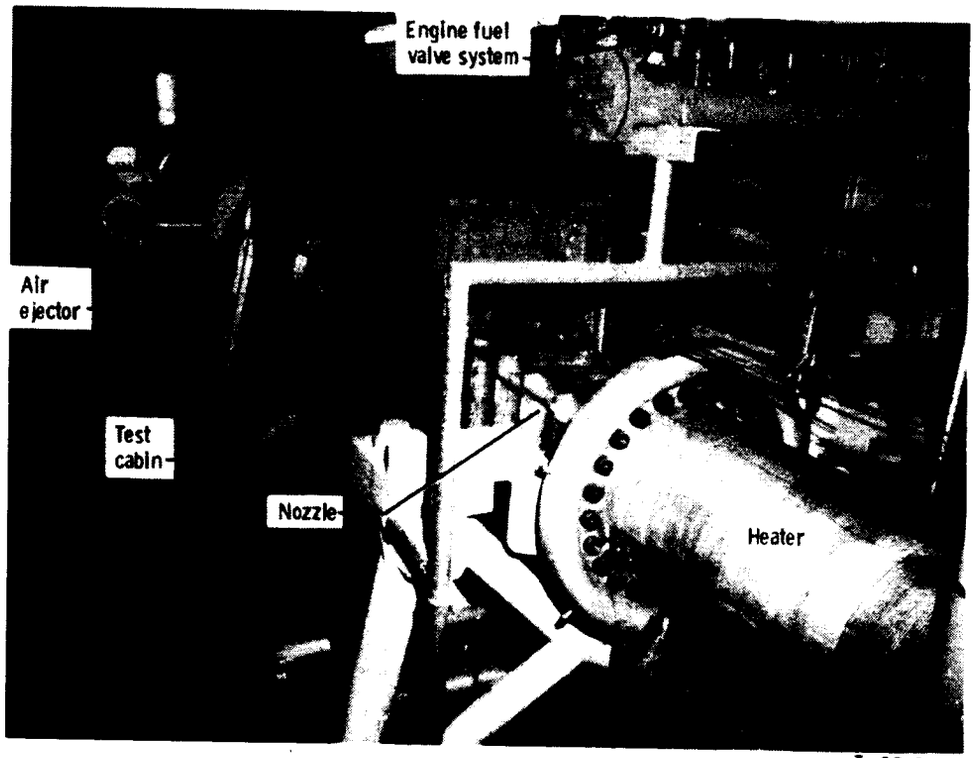

L-82-3469

(a) Overall view.

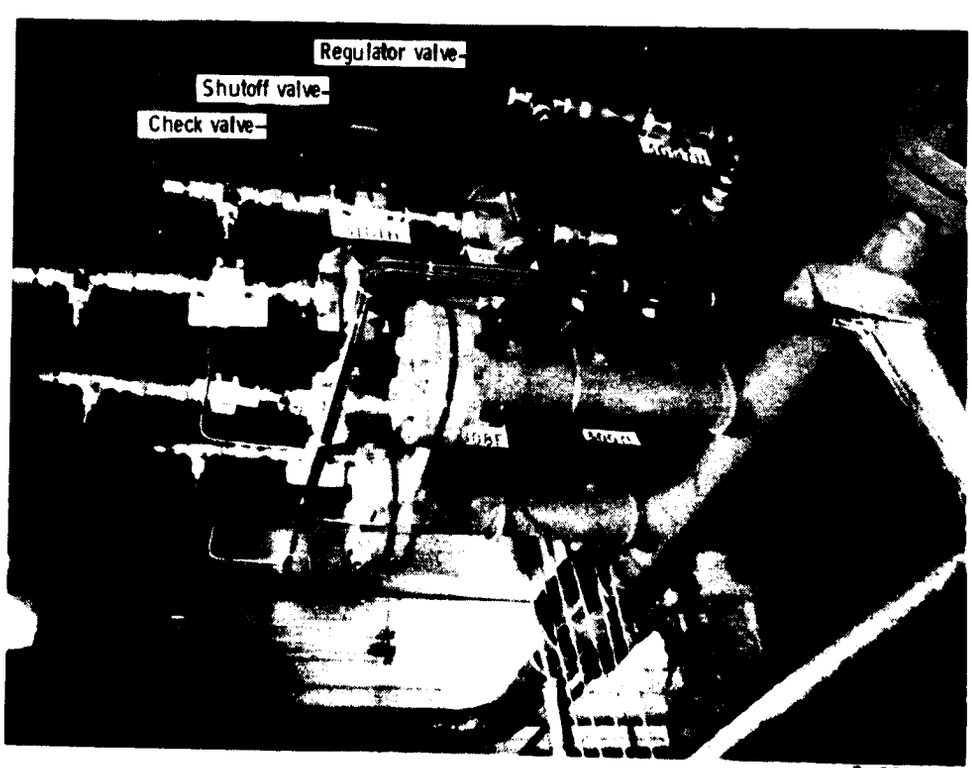

L-82-3464

(b) Engine fuel supply and control system.

Figure 5. Langley Mach 4 Scramjet Test Facility.

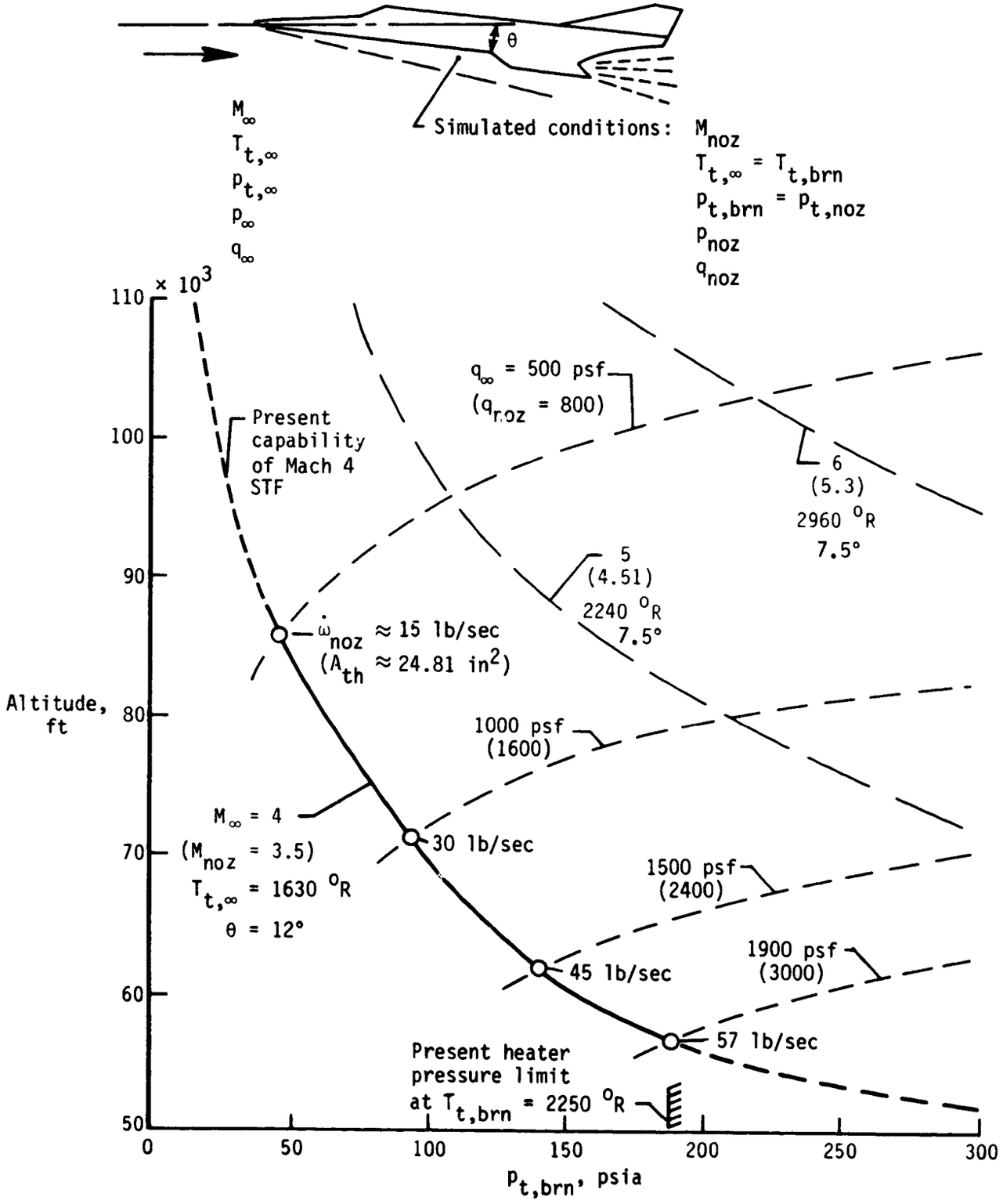

Figure 6. Simulated flight conditions.

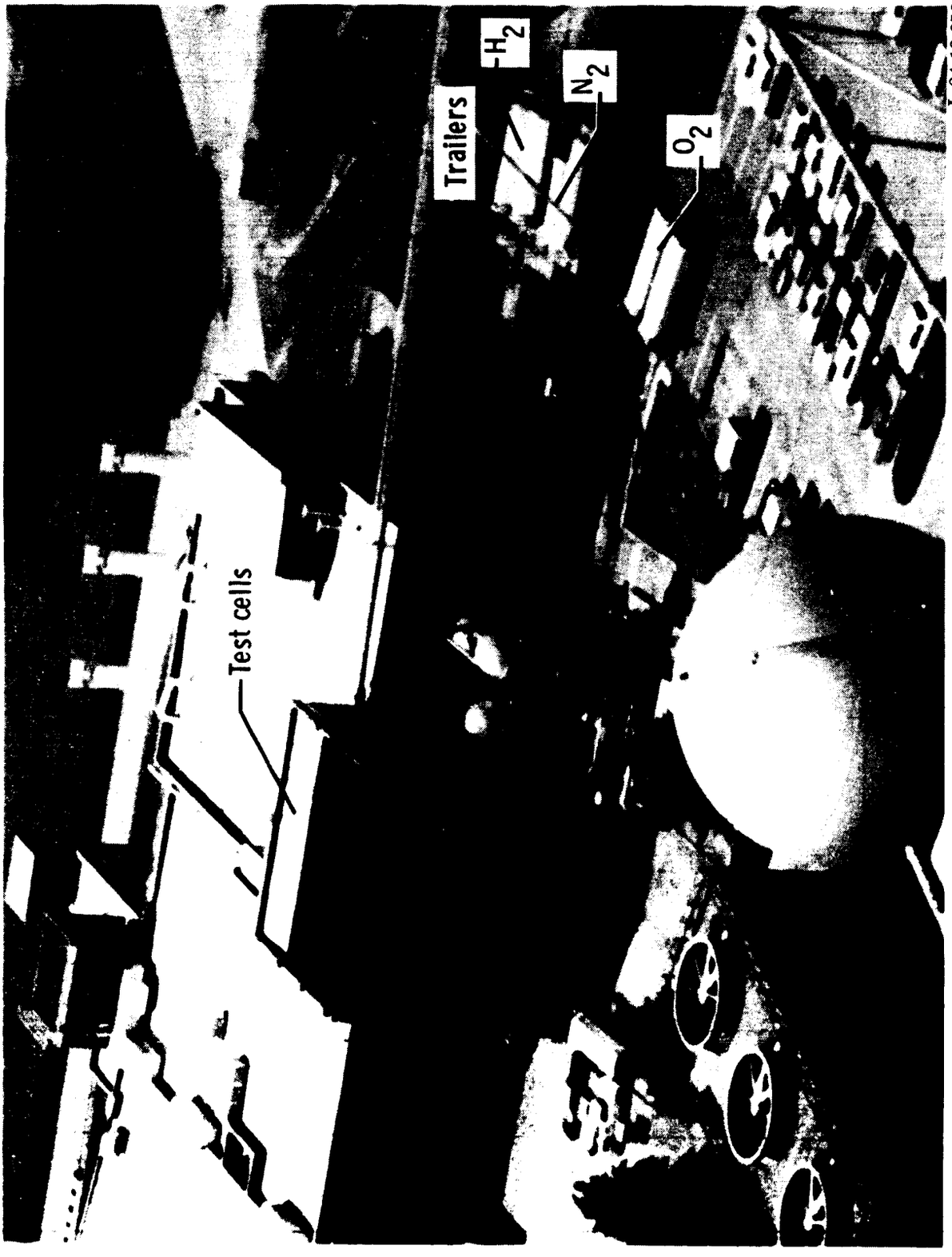

Figure 7. Test cell complex.

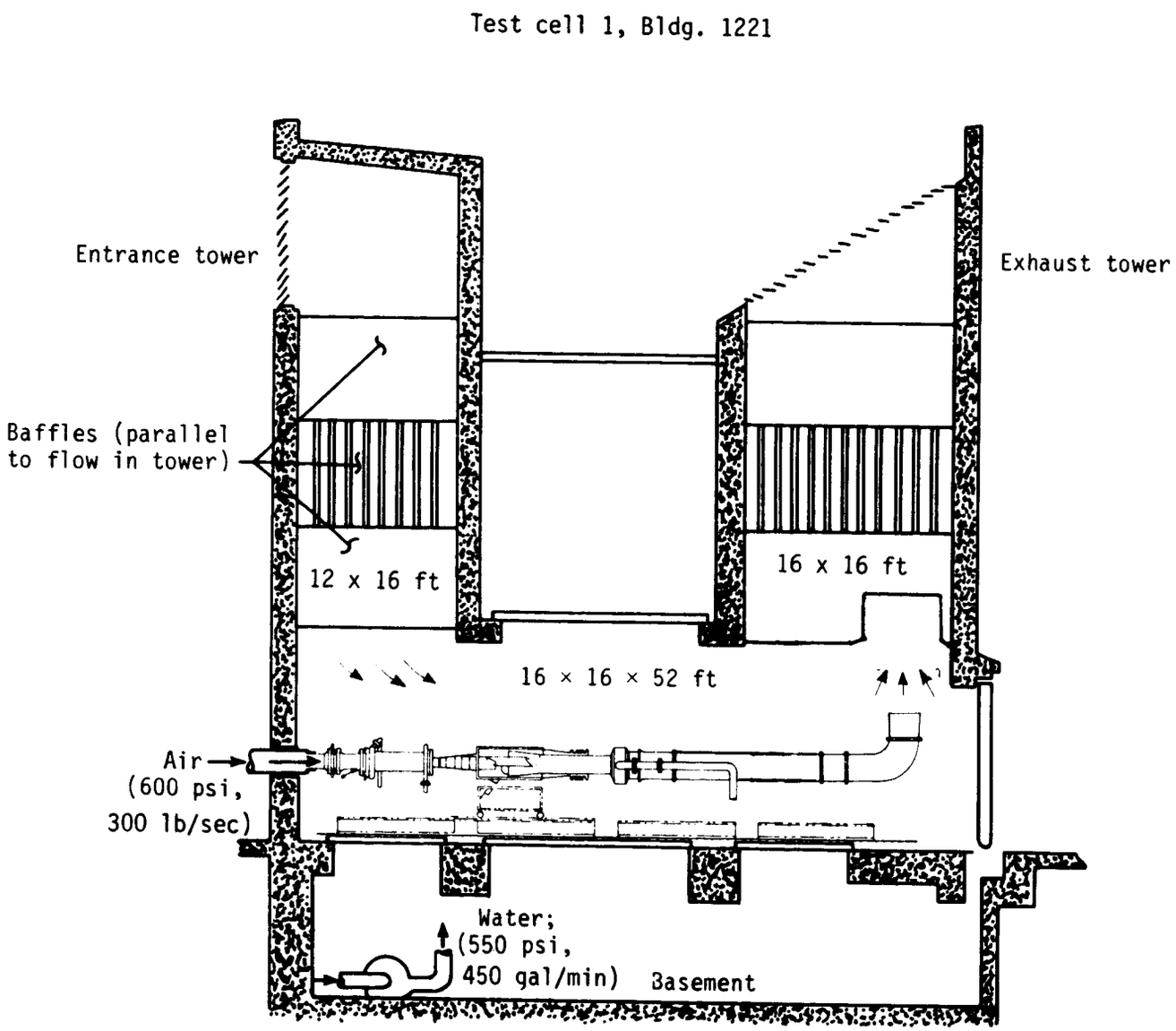

Figure 8. Cross-sectional view of test cell.

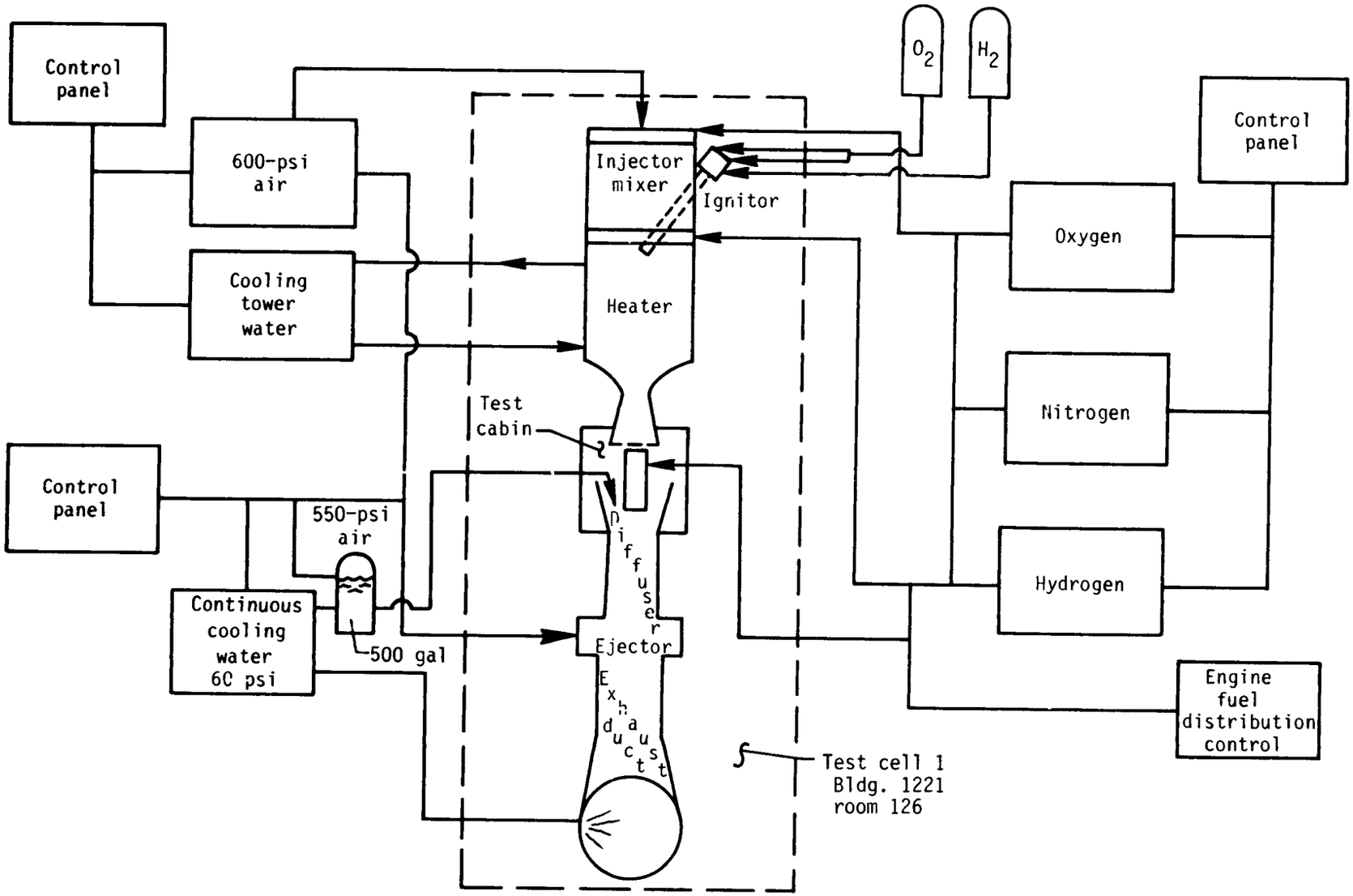

Figure 9. Langley Mach 4 Scramjet Test Facility systems and controls.

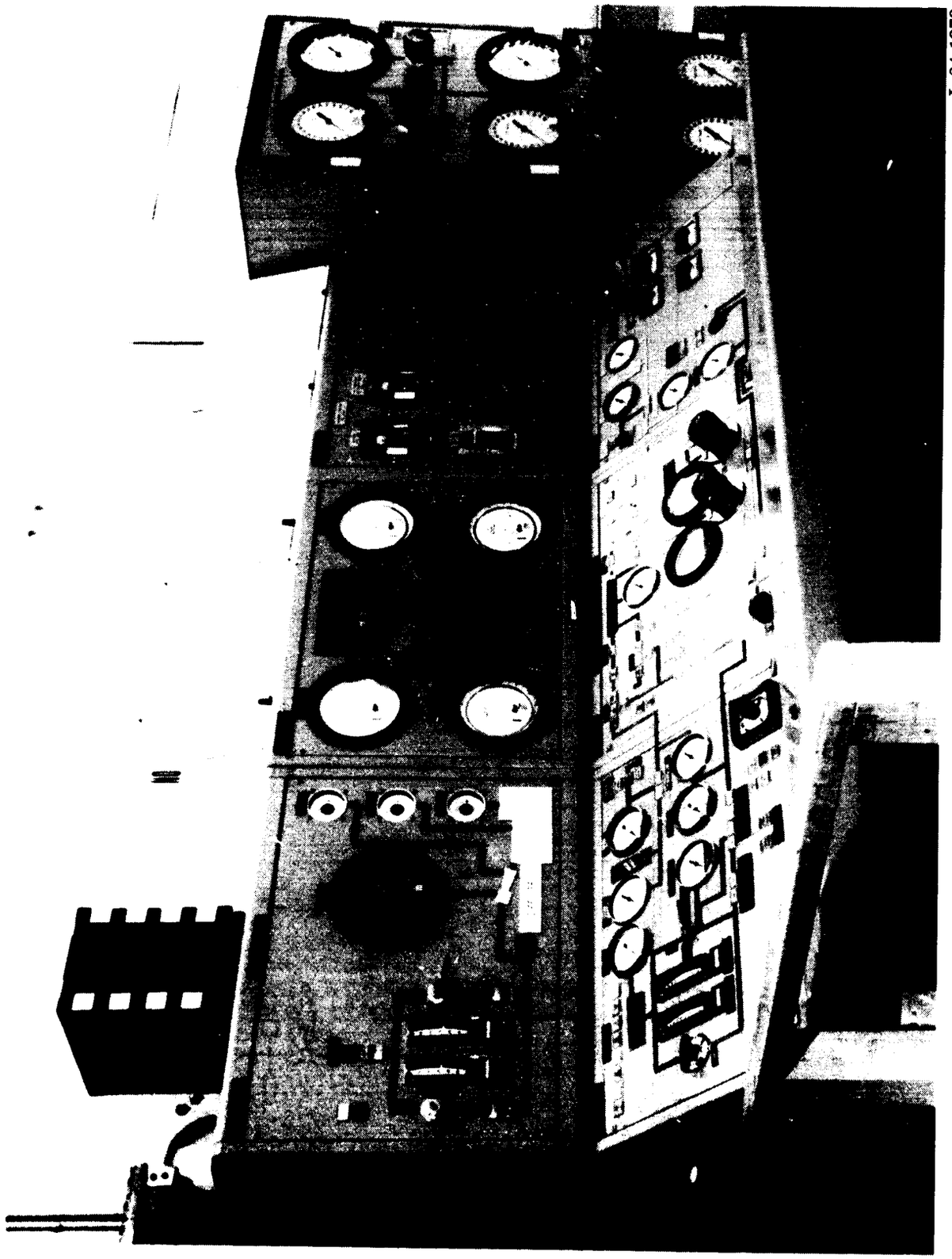

L-84-1970

Figure 10. Langley Mach 4 Scramjet Test Facility control room.

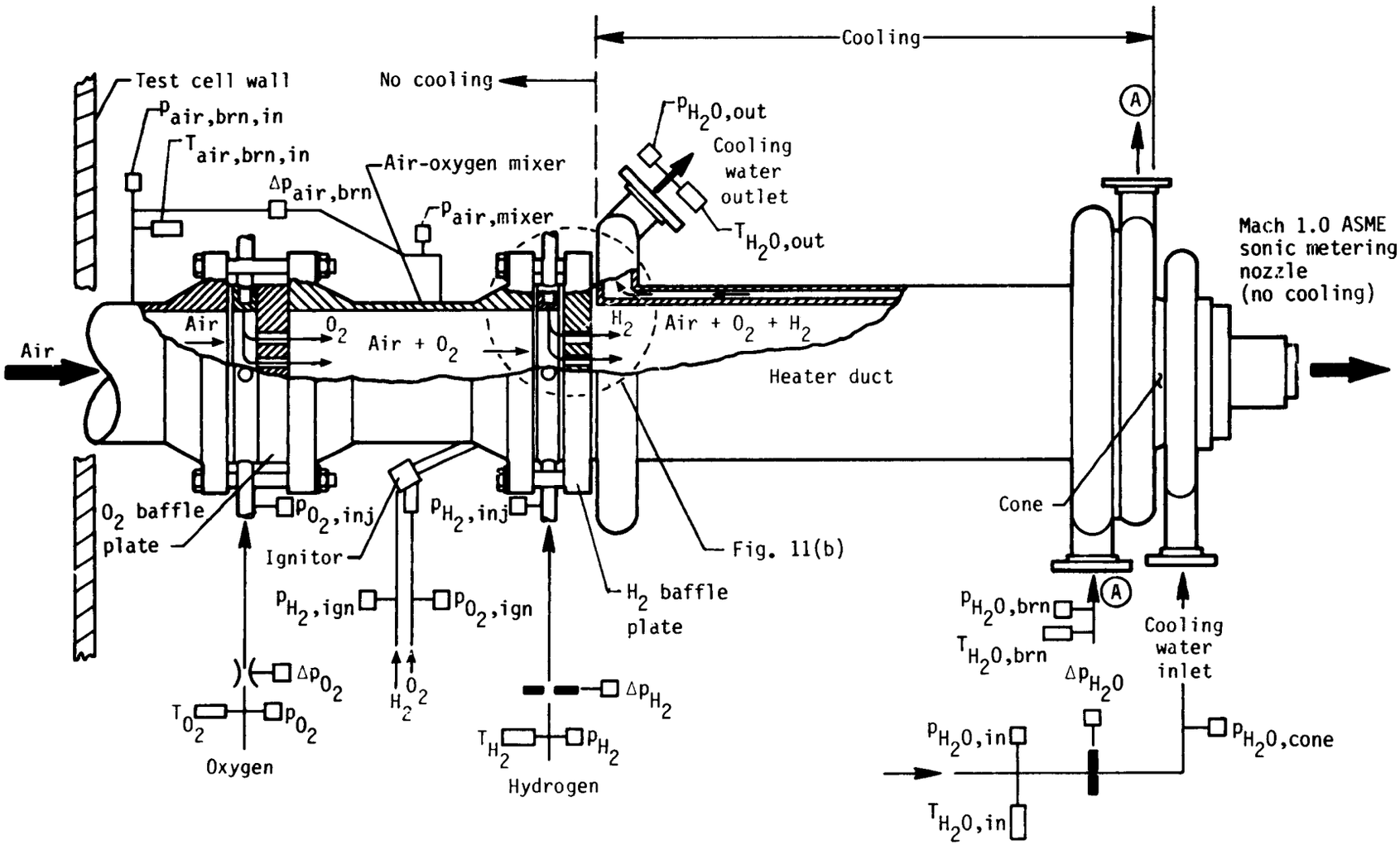

(a) Setup for airflow calibration and heater performance tests.

Figure 11. Mixer and heater assembly.

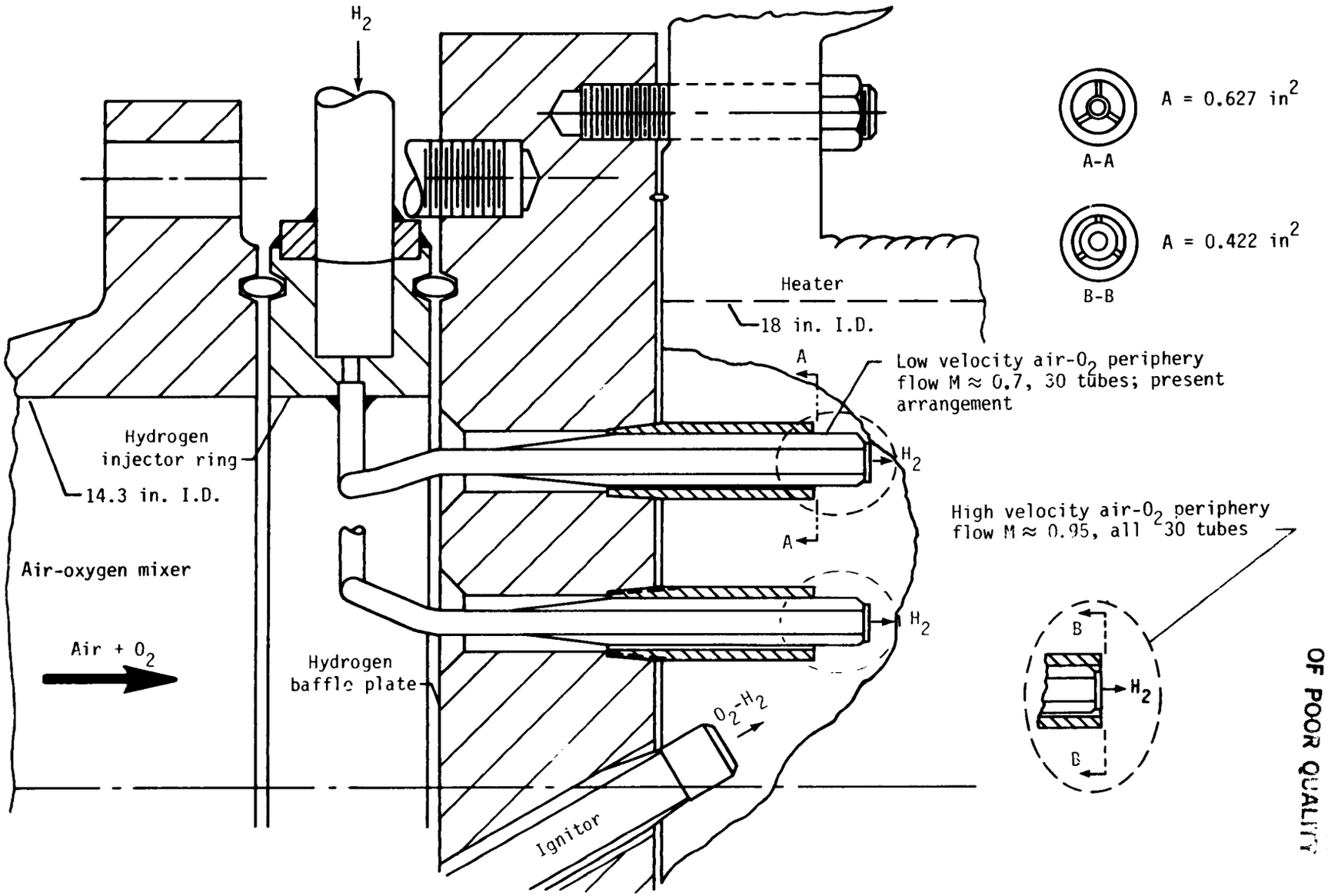

(b) Details of heater hydrogen injector.

Figure 11. Concluded.

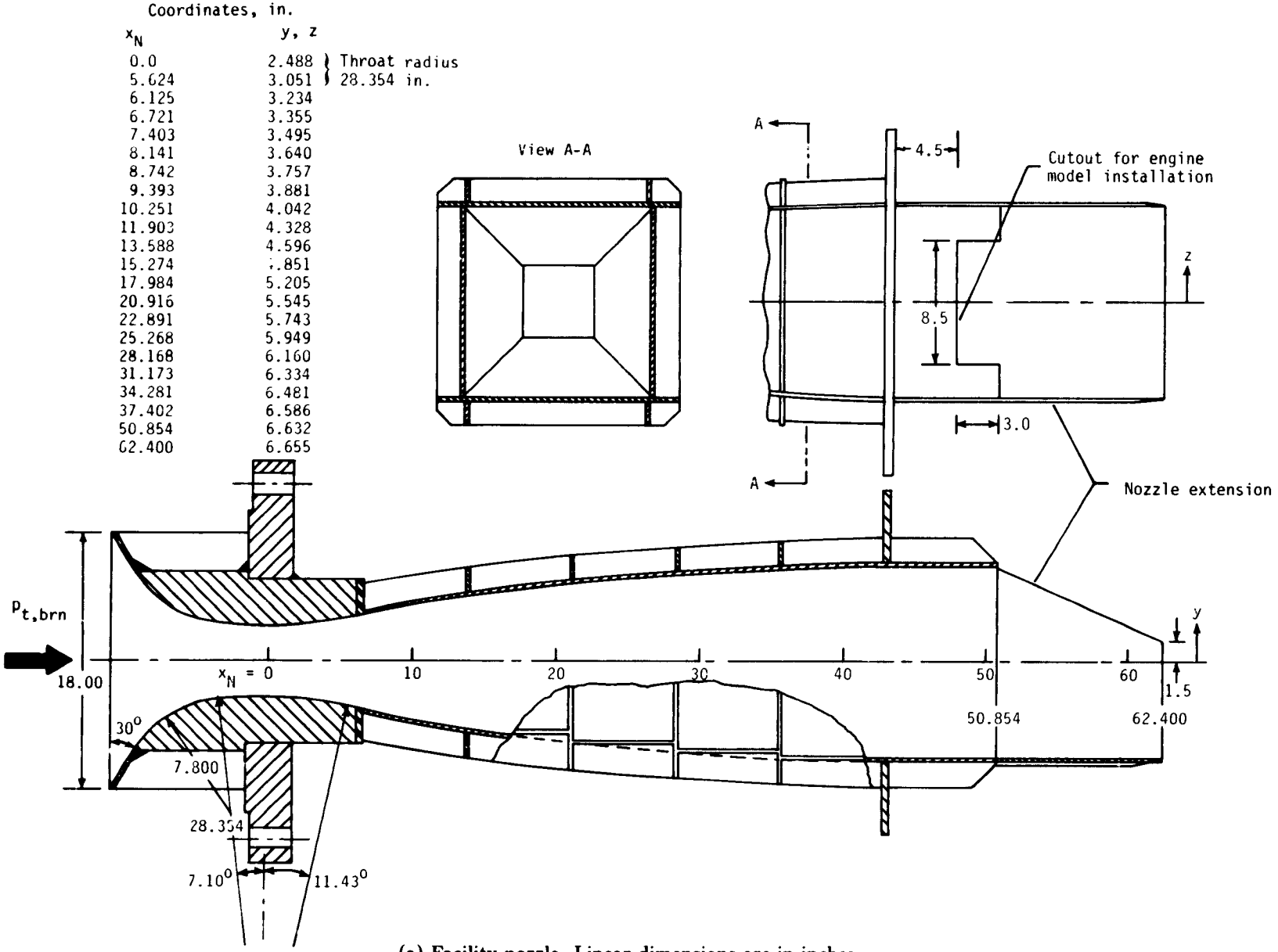

(a) Facility nozzle. Linear dimensions are in inches.

Figure 12. Nozzles used during Mach 4 STF calibration and checkout tests.

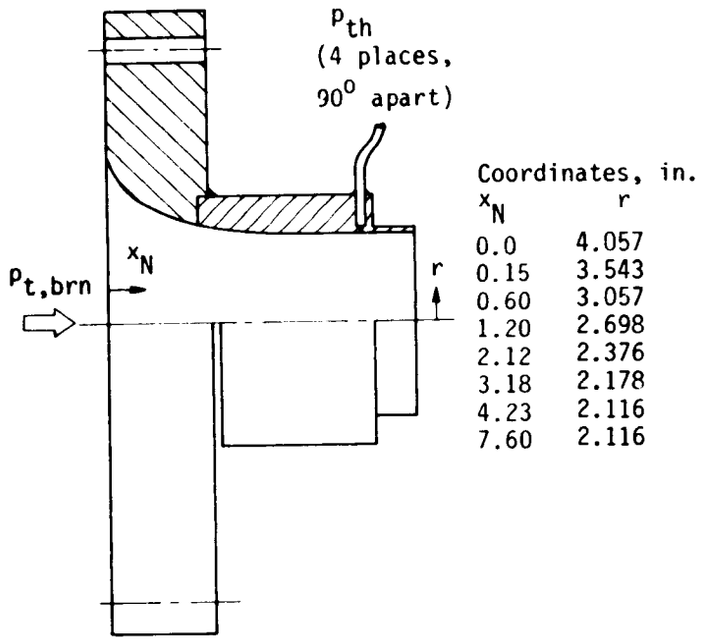

Coordinates, in.

x_N	r
0.0	4.057
0.15	3.543
0.60	3.057
1.20	2.698
2.12	2.376
3.18	2.178
4.23	2.116
7.60	2.116

(b) Mach 1.0 ASME sonic metering nozzle; unheated airflow calibration tests.

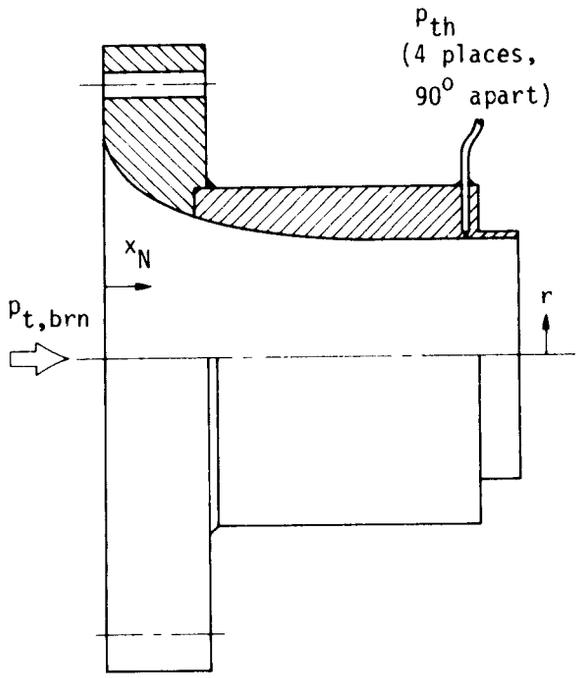

Coordinates, in.

x_N	r
0.00	5.387
0.20	4.704
0.80	4.060
1.60	3.583
2.80	3.155
4.20	2.892
5.60	2.810
10.00	2.810

(c) Mach 1.0 ASME sonic metering nozzle; heated airflow calibration tests.

Figure 12. Concluded.

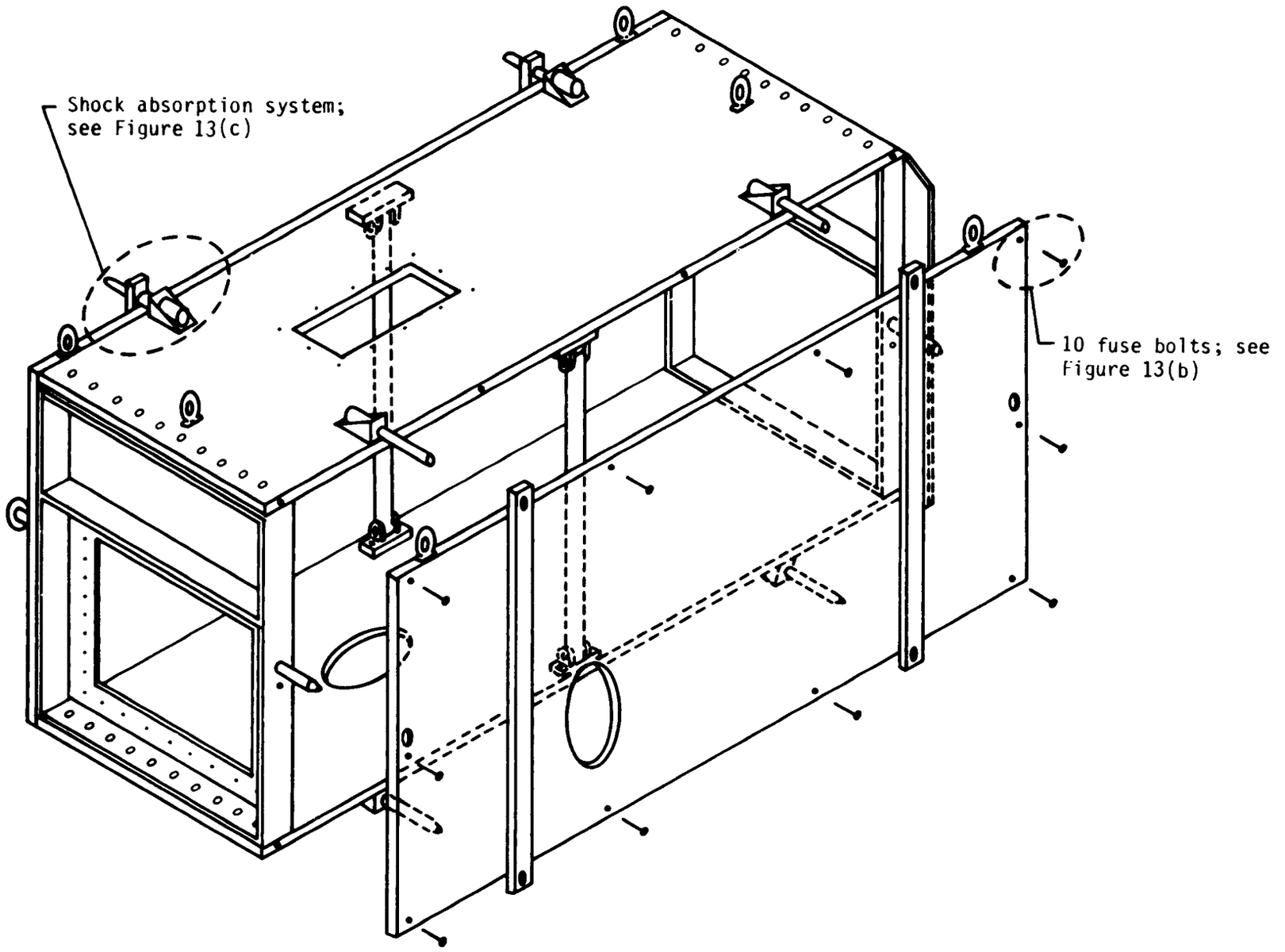

(a) Overall view.

Figure 13. Test cabin details.

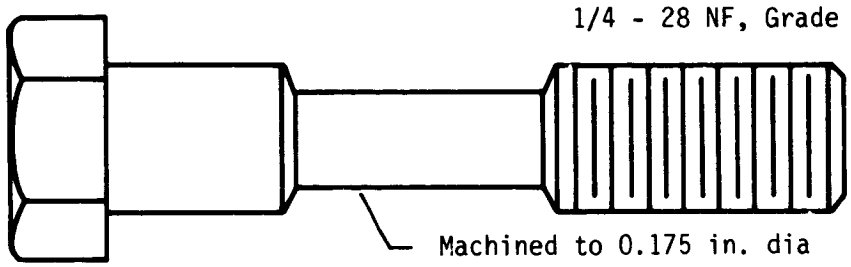

(b) Sidewall fuse bolts.

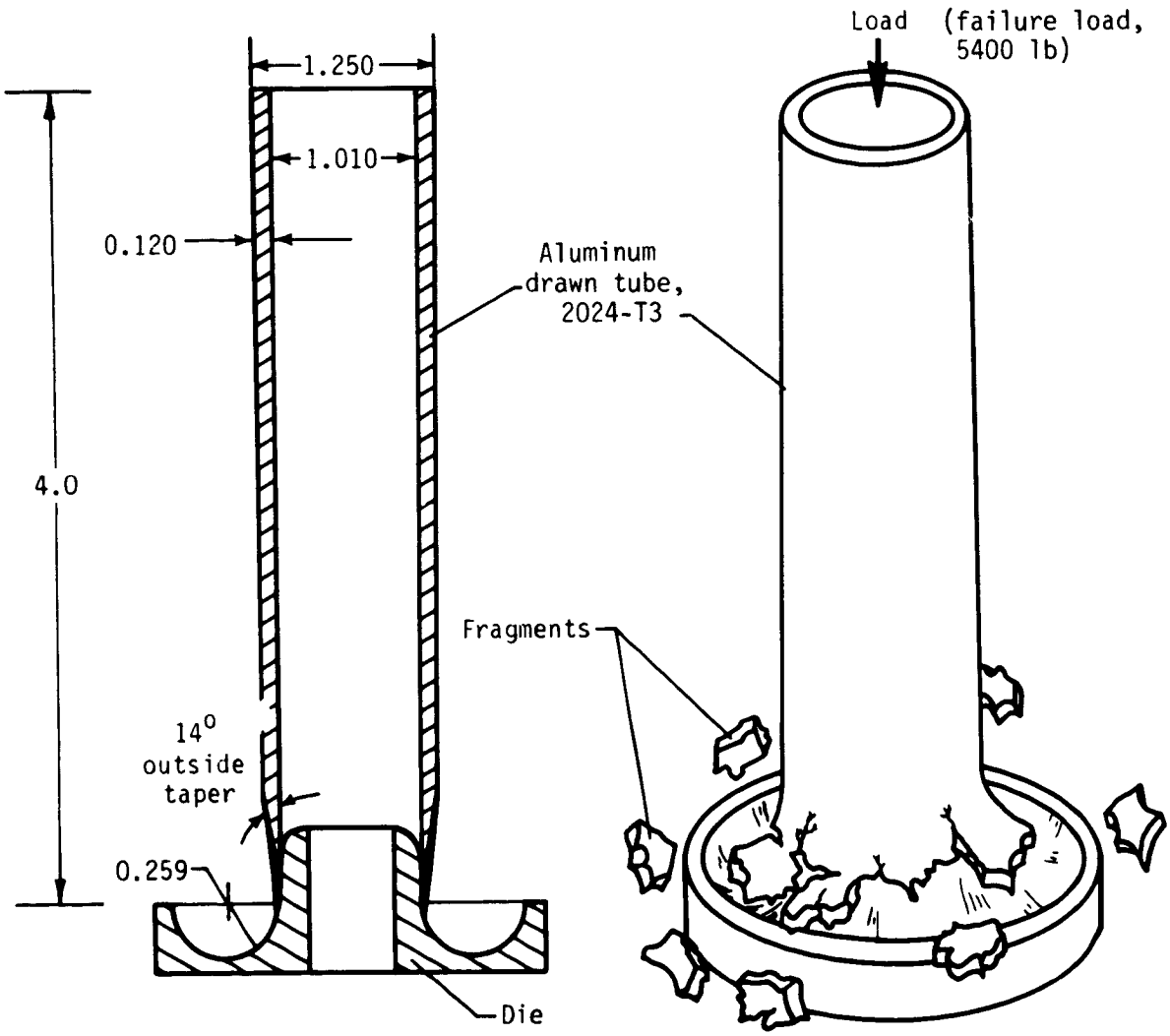

(c) Side wall shock absorption system; details and sketch illustrating fragmenting process (ref. 41). Linear dimensions are in inches.

Figure 13. Concluded.

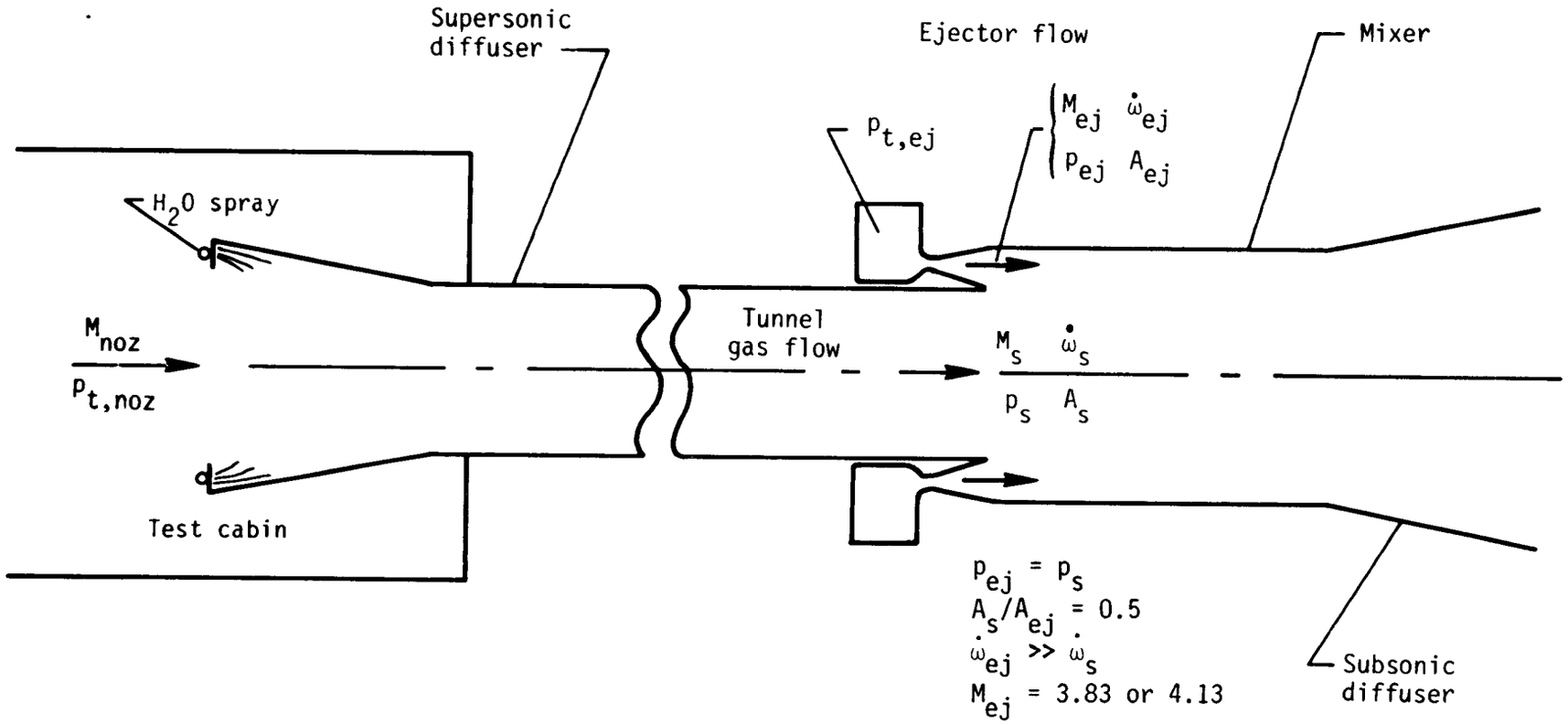

Figure 14. Air-ejector schematic.

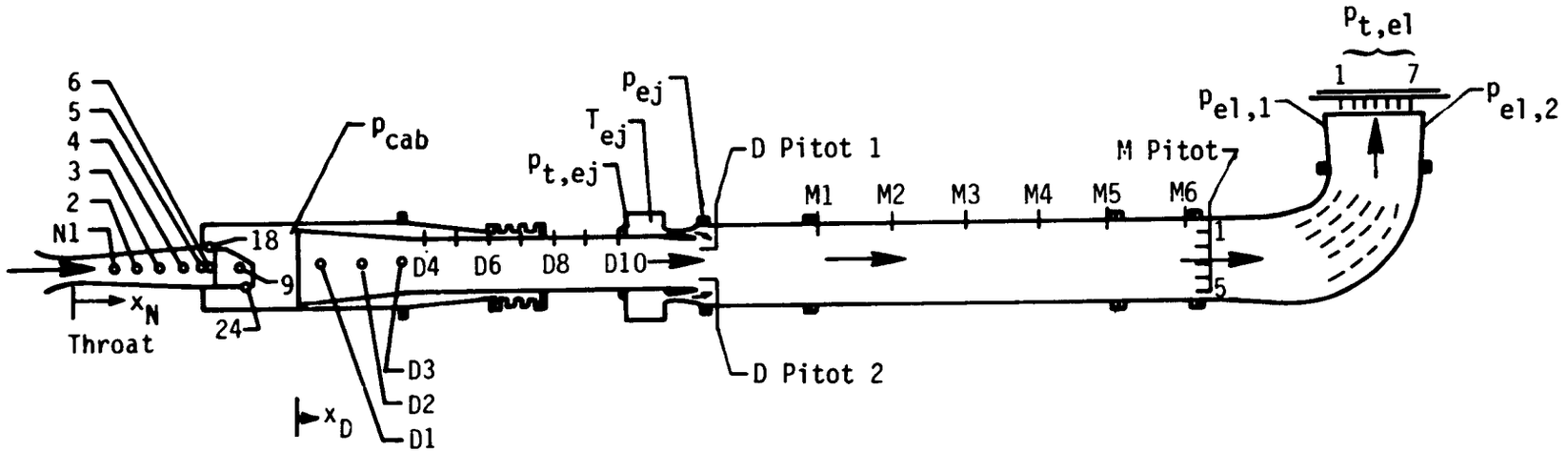

Nozzle orifices

x_N, in.		
16.60	N1	
24.10	2	Side
31.60	3	Side
39.10	4	Side
45.85	5	Side
48.35	6	Side
61.40	9	Side
48.35	18	Top
61.40	24	Bottom

Diffuser orifices

x_D, in.		
7.5	D1	
21.0	2	Side
34.5	3	Side
42.0	4	Top
52.5	5	Top
63.0	6	Top
73.5	7	Top
84.0	8	Top
94.5	9	Top
105.0	10	
136.0	D Pitot	

Mixer orifices

x_D, in.	
176.00	M1
199.75	2
223.50	3
247.25	4
271.00	5
295.00	6
297.00	M Pitot

Figure 15. Facility instrumentation locations.

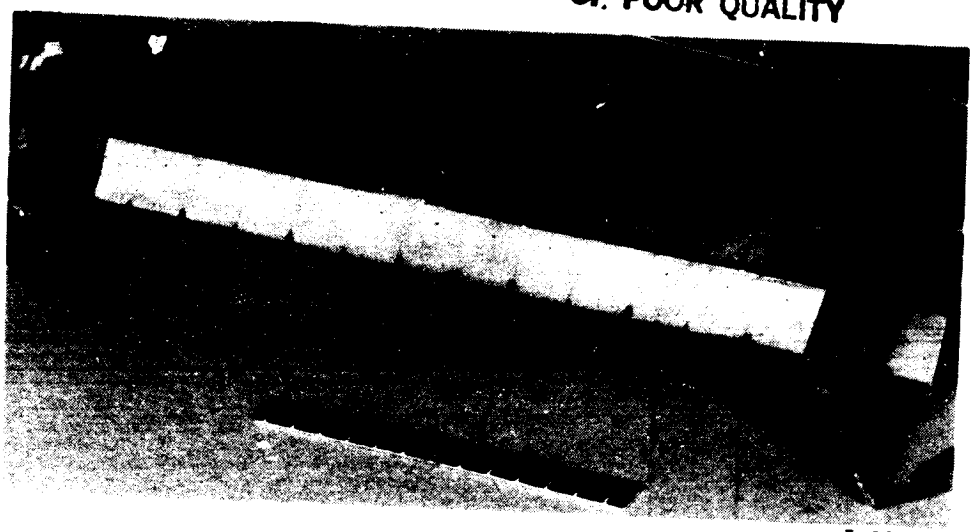

L-82-4365

(a) Pitot-pressure and total-temperature rake.

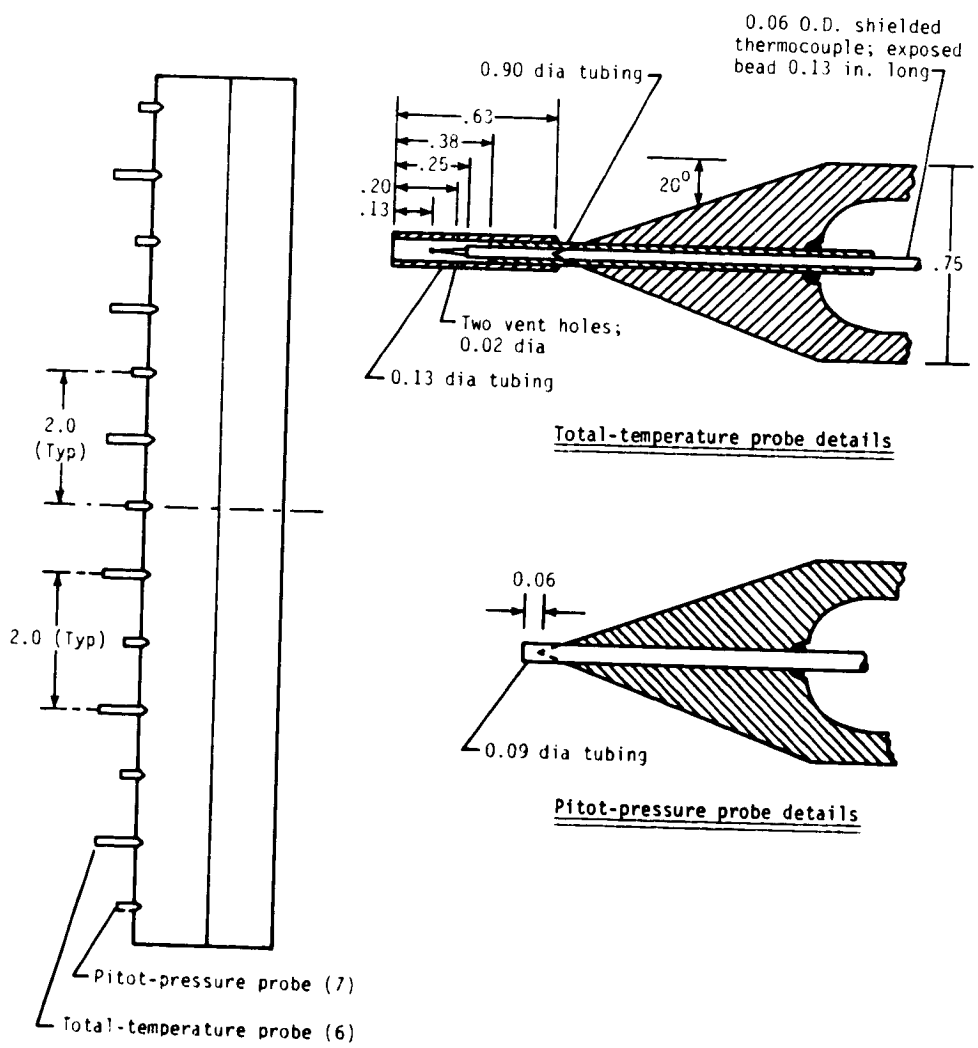

(b) Details of the pitot-pressure and total-temperature rake.

Figure 16. Nozzle-exit survey rakes. Linear dimensions are in inches.

L-82-4362

(c) Static-pressure rake.

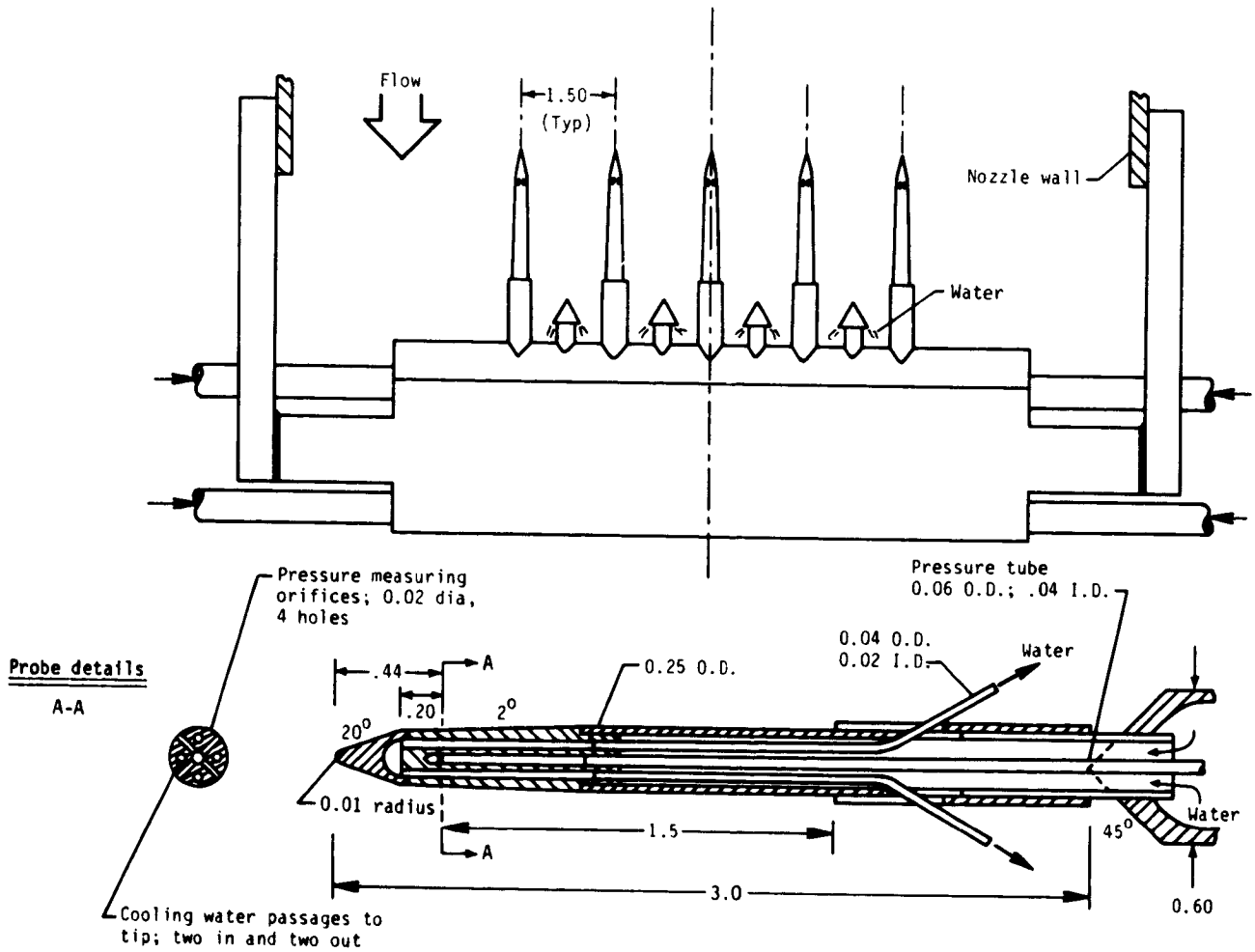

(d) Details of the static-pressure rake.

Figure 16. Continued.

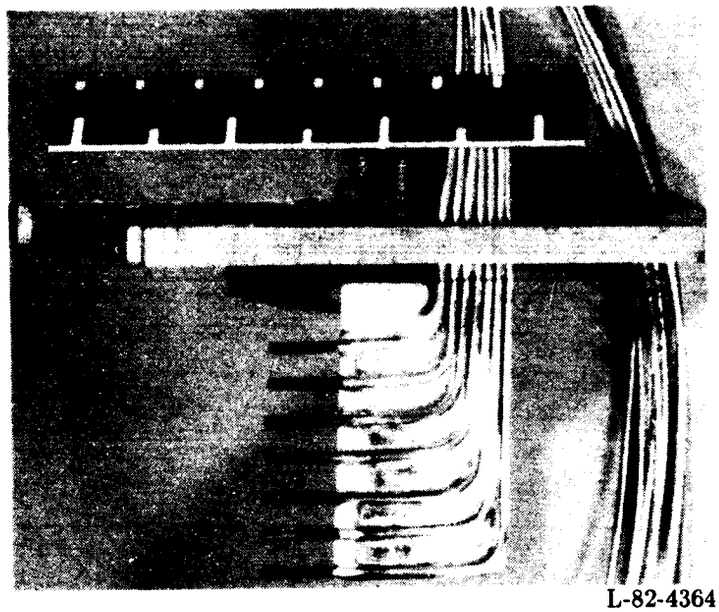

L-82-4364

(e) Boundary-layer pitot-pressure rake.

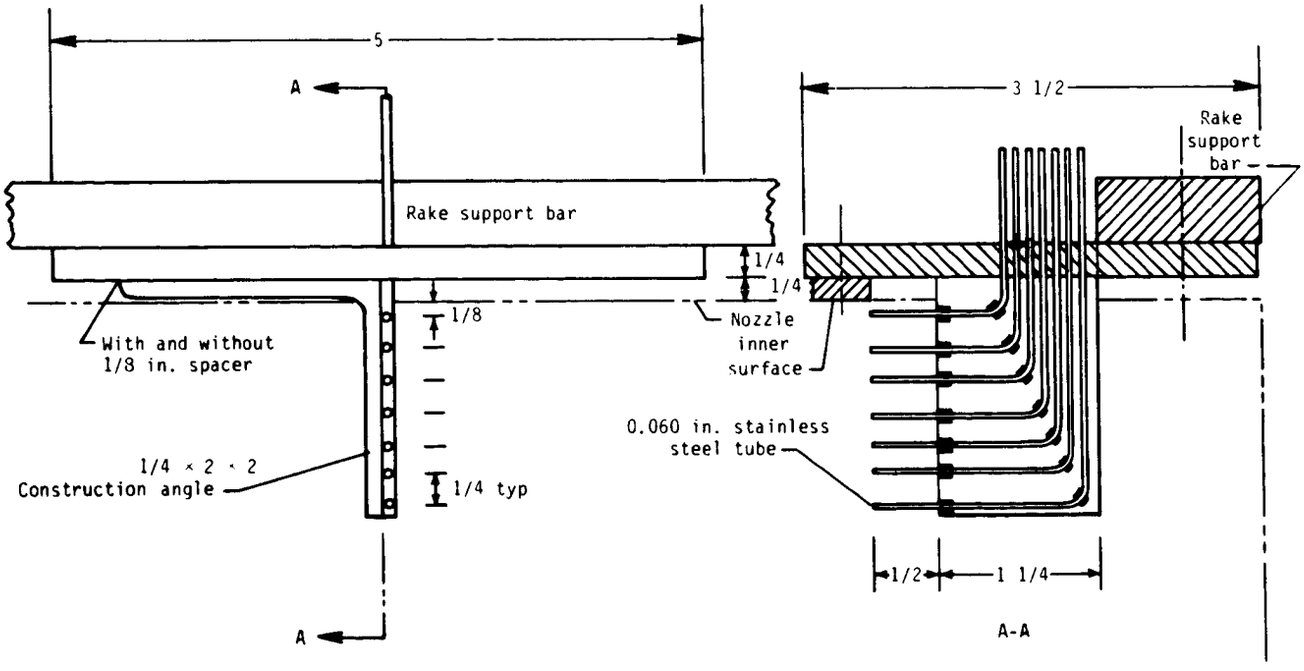

(f) Details of the boundary-layer pitot-pressure rake.

Figure 16. Continued.

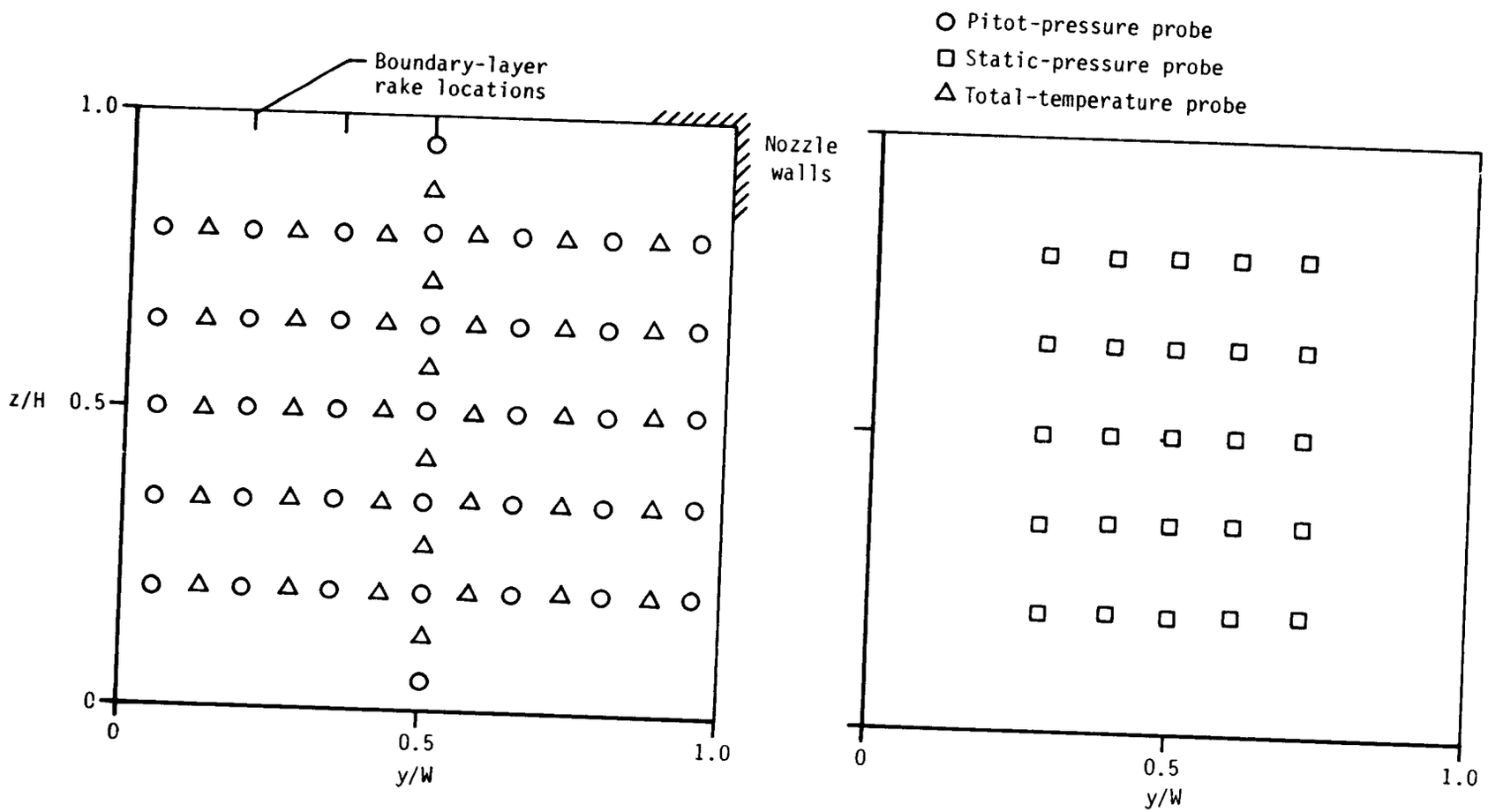

(g) Probe locations; H = W = 13.264 in.

Figure 16. Concluded.

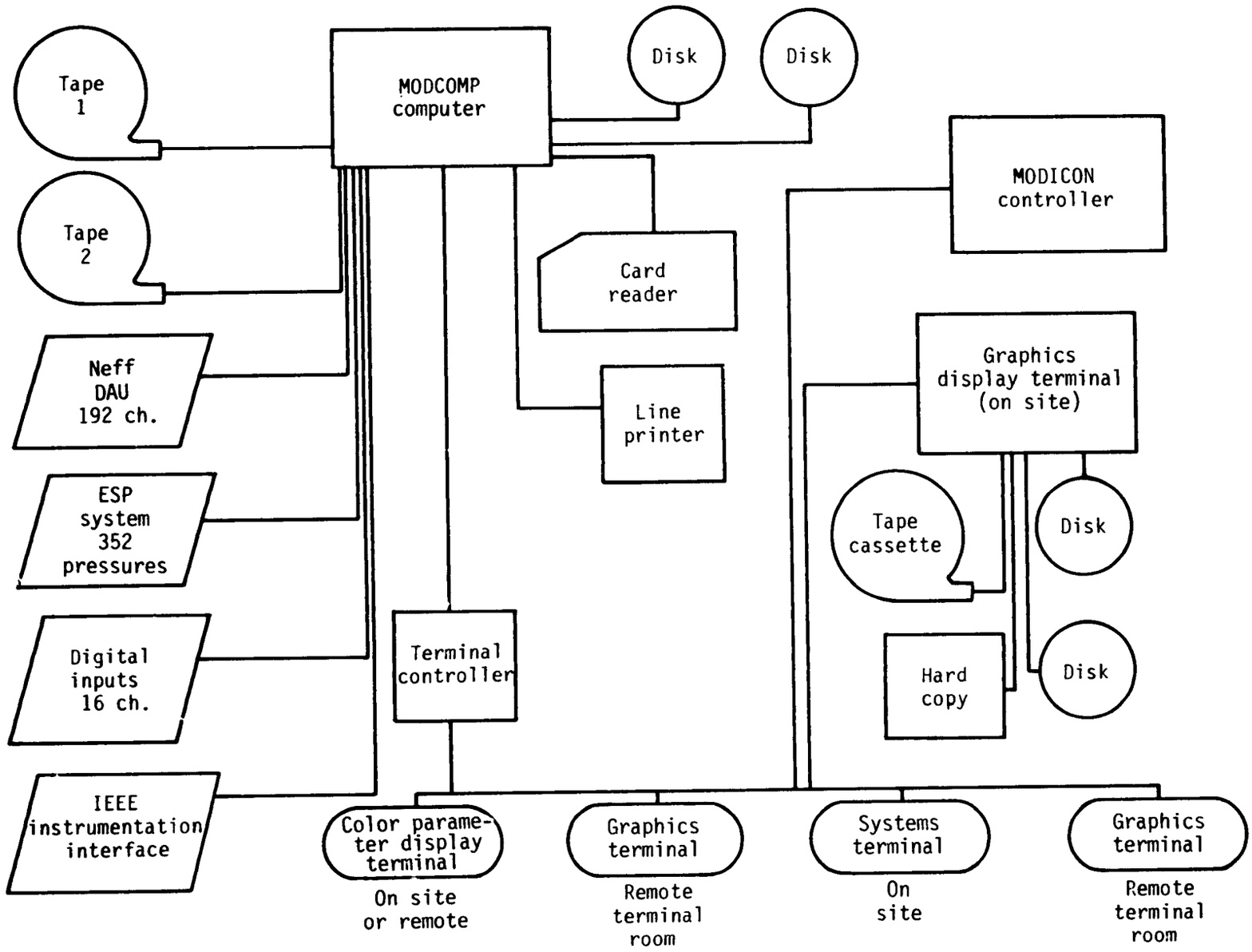

(a) Hardware schematic.

Figure 17. Data acquisition system, located in control room.

L-81-6056

(b) Photograph of data acquisition system.

Figure 17. Concluded.

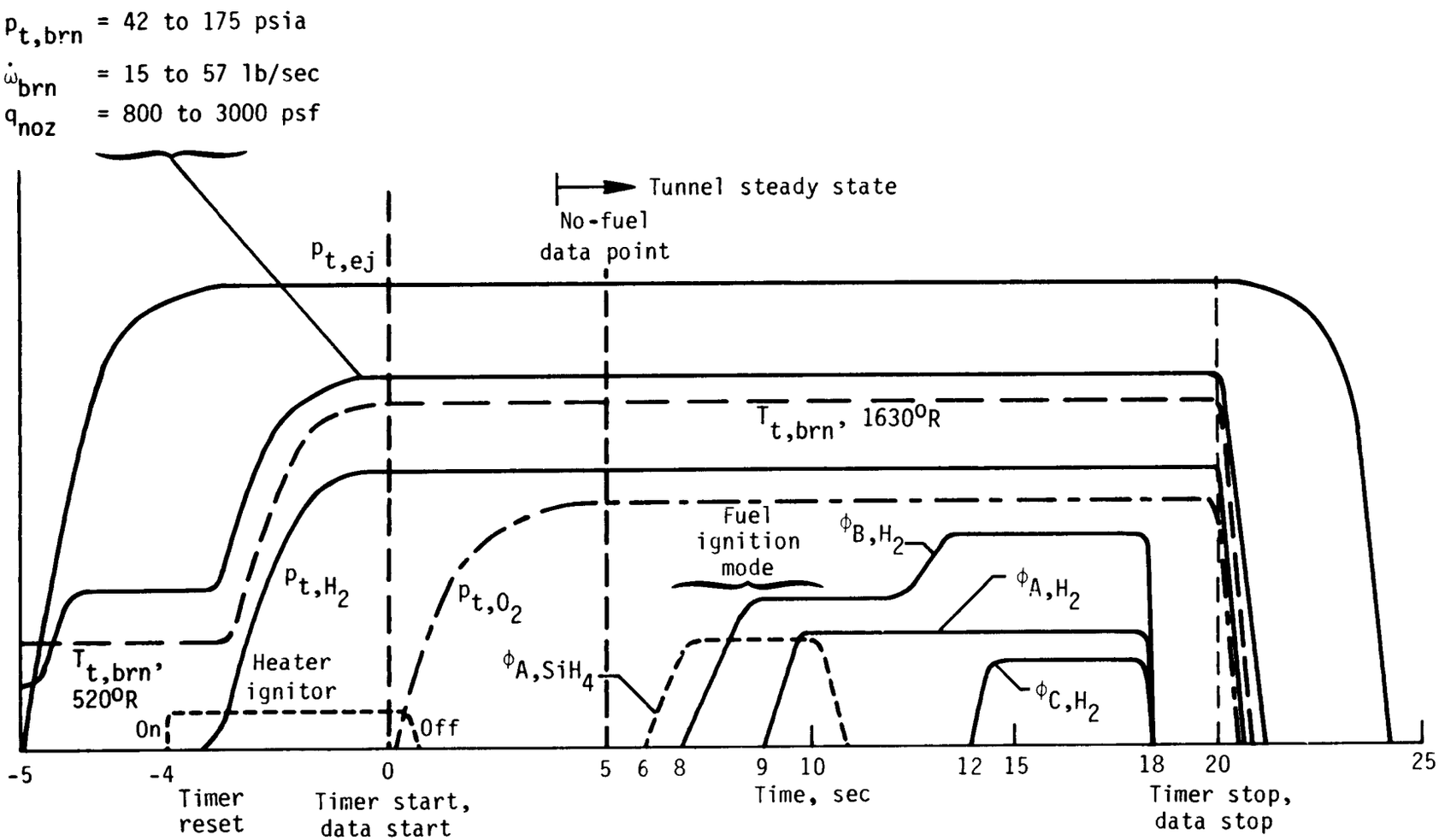

Figure 18. A typical test sequence of the Langley Mach 4 Scramjet Test Facility.

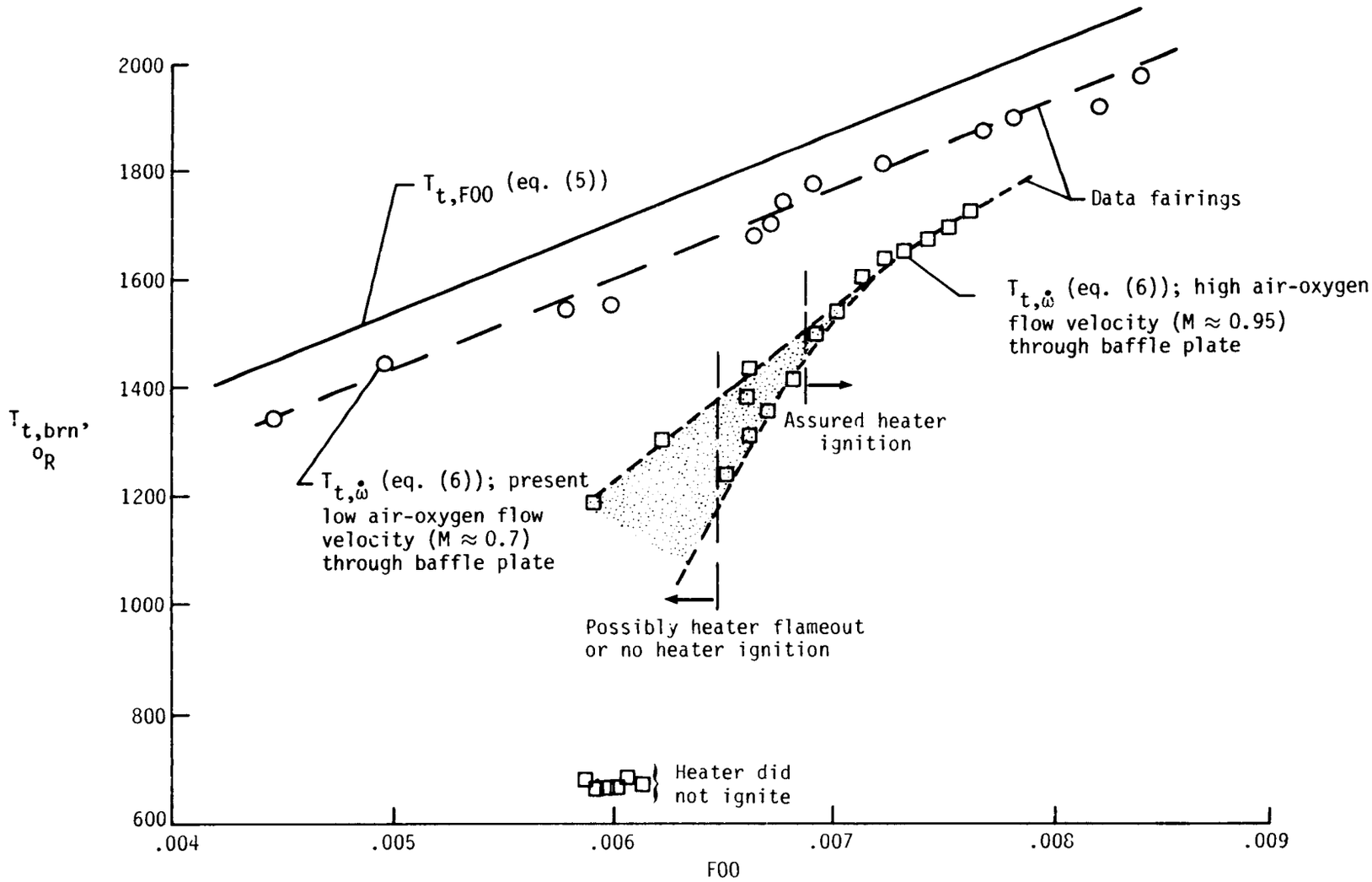

Figure 19. Facility stream total temperature as affected by heater velocity.

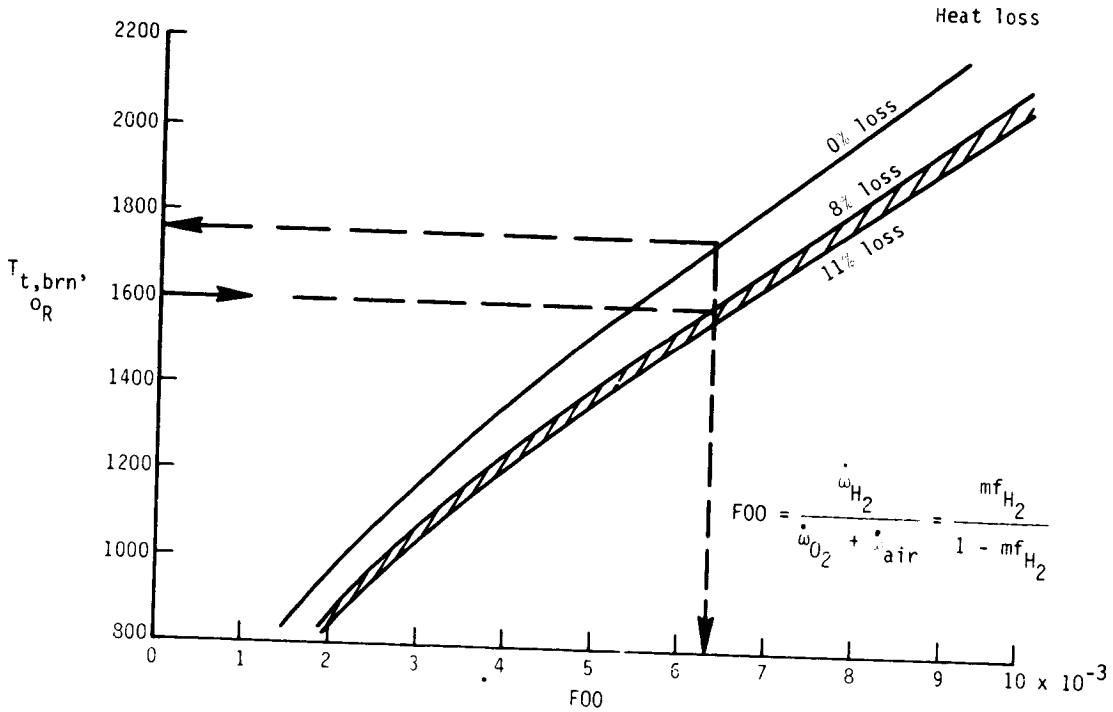

(a) Mixture ratio of hydrogen mass flow to oxygen and air mass flow FOO.

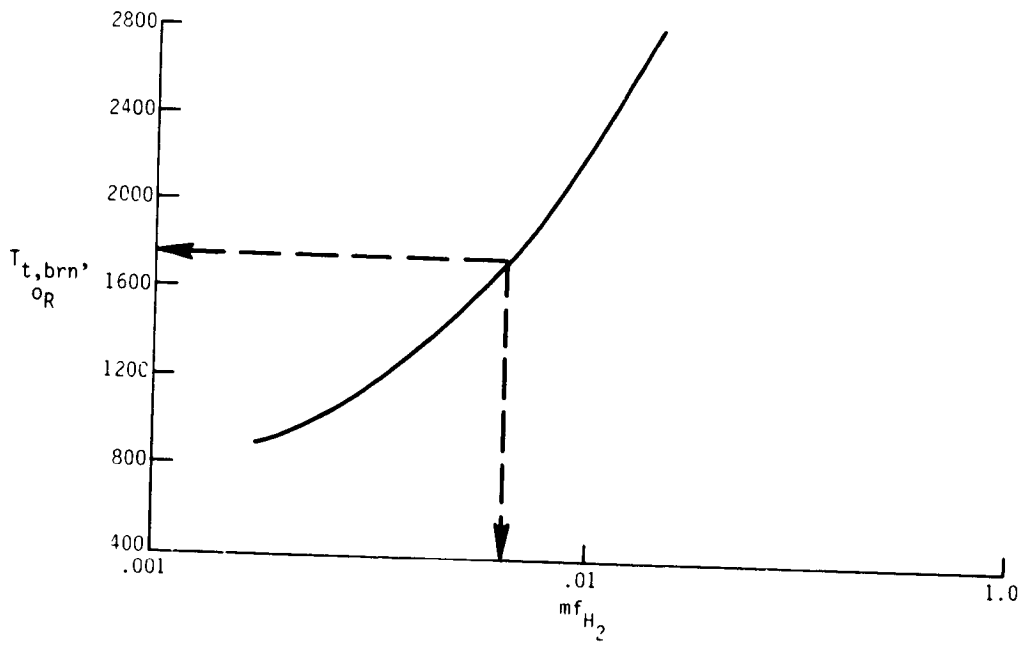

(b) Mass fraction of hydrogen.

Figure 20. Parameters of hydrogen burning in air with oxygen replenishment to yield vitiated simulated air.

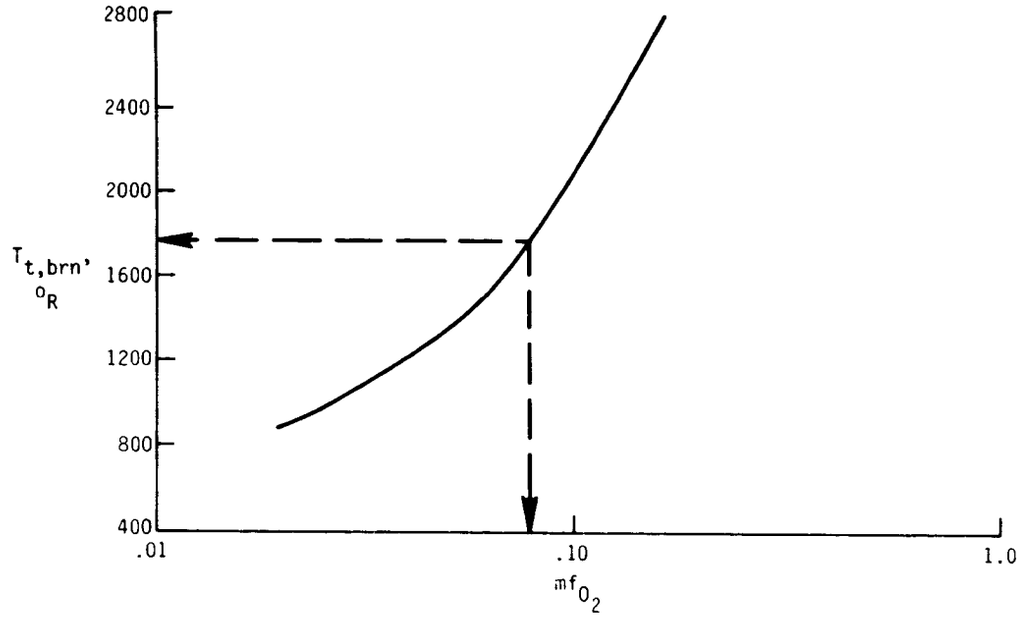

(c) Mass fraction of oxygen.

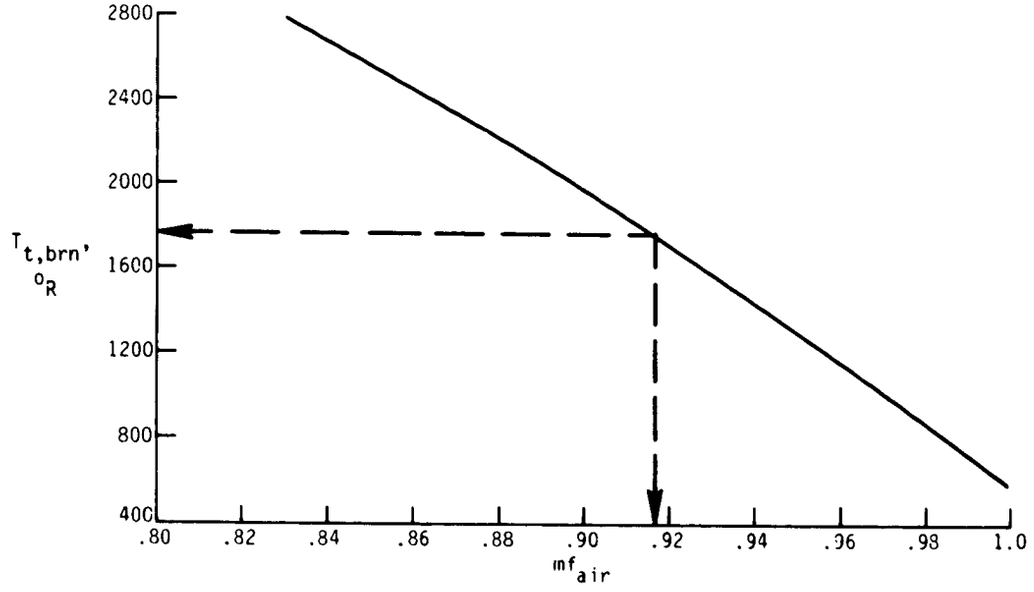

(d) Mass fraction of air.

Figure 20. Concluded.

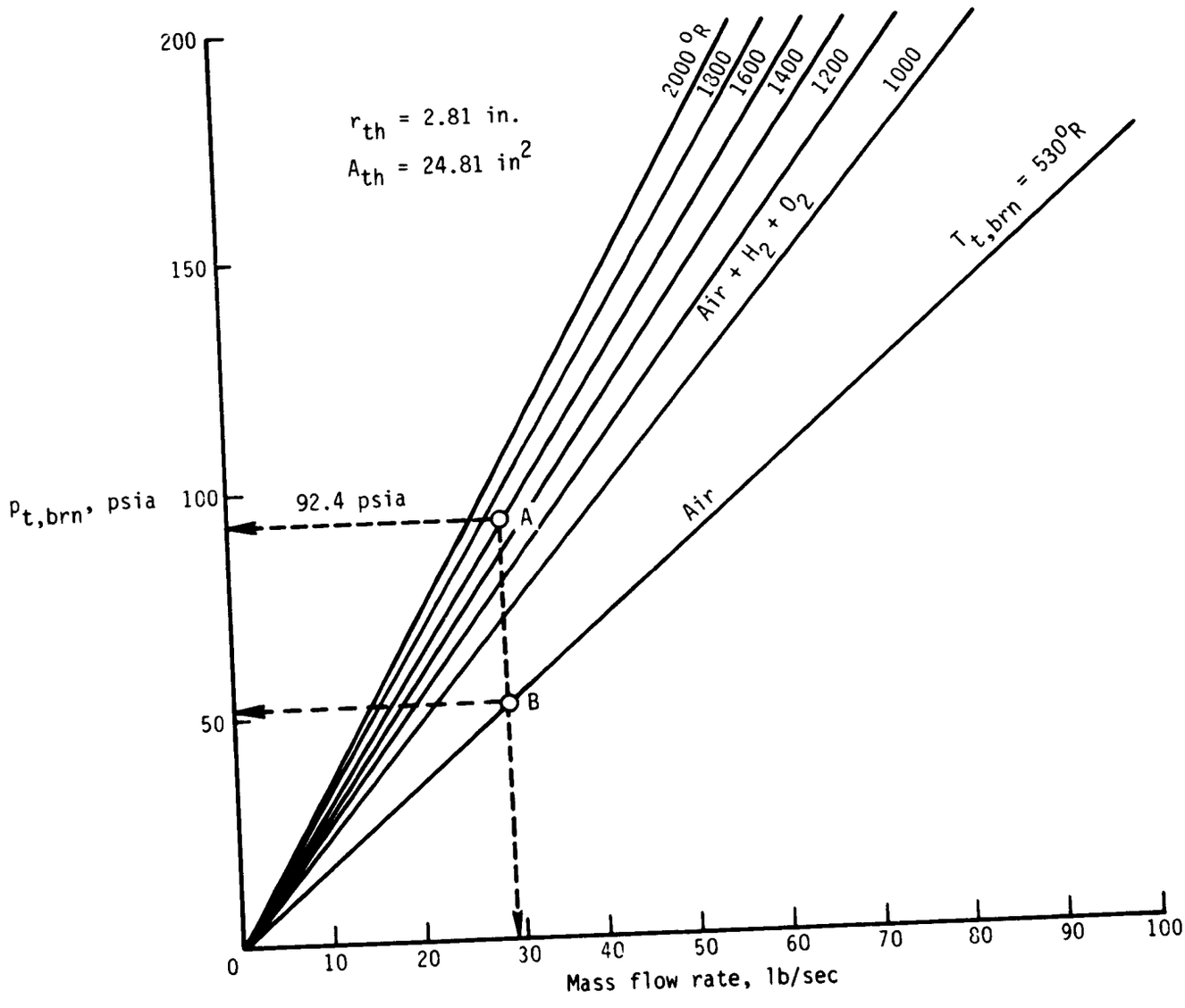

Figure 21. General operational parameters for a nozzle with a throat area of 24.81 in^2.

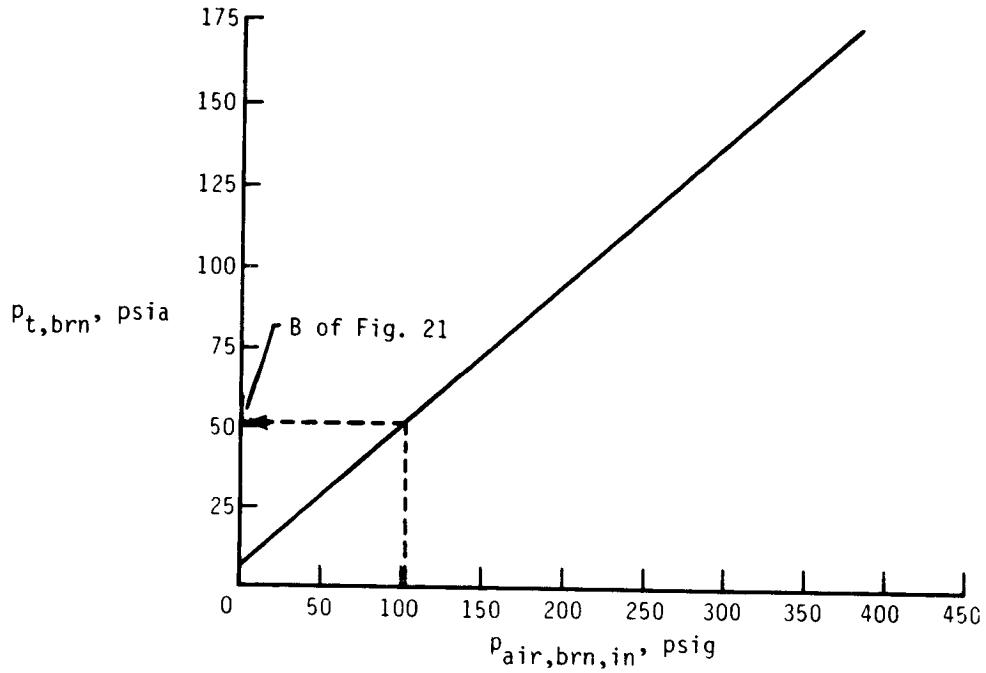

(a)Unheated airflow. $T_{t,brn} = 520°R$.

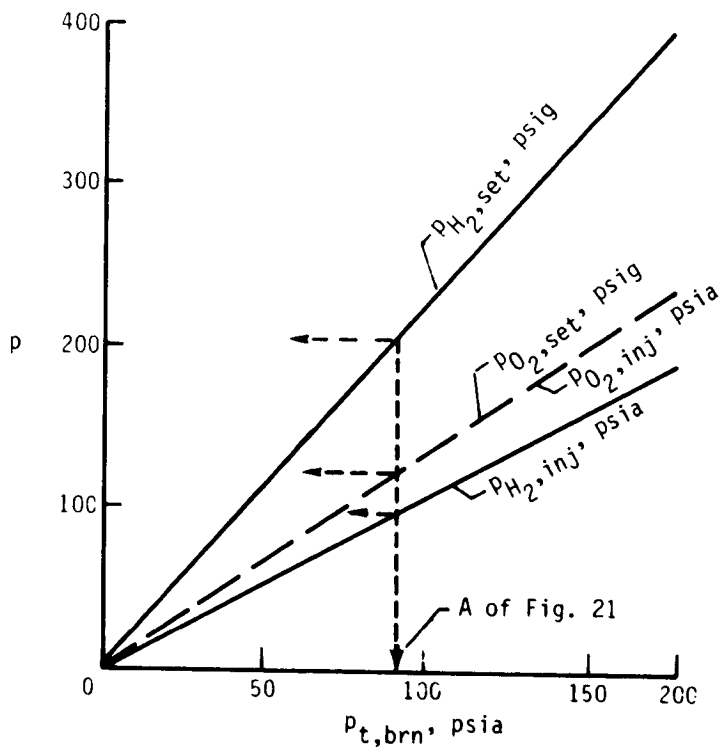

(b) Hydrogen and oxygen pressures correlated with heater total pressures. $T_{t,brn} = 1630°R$.

Figure 22. Langley Mach 4 Scramjet Test Facility operational pressures.

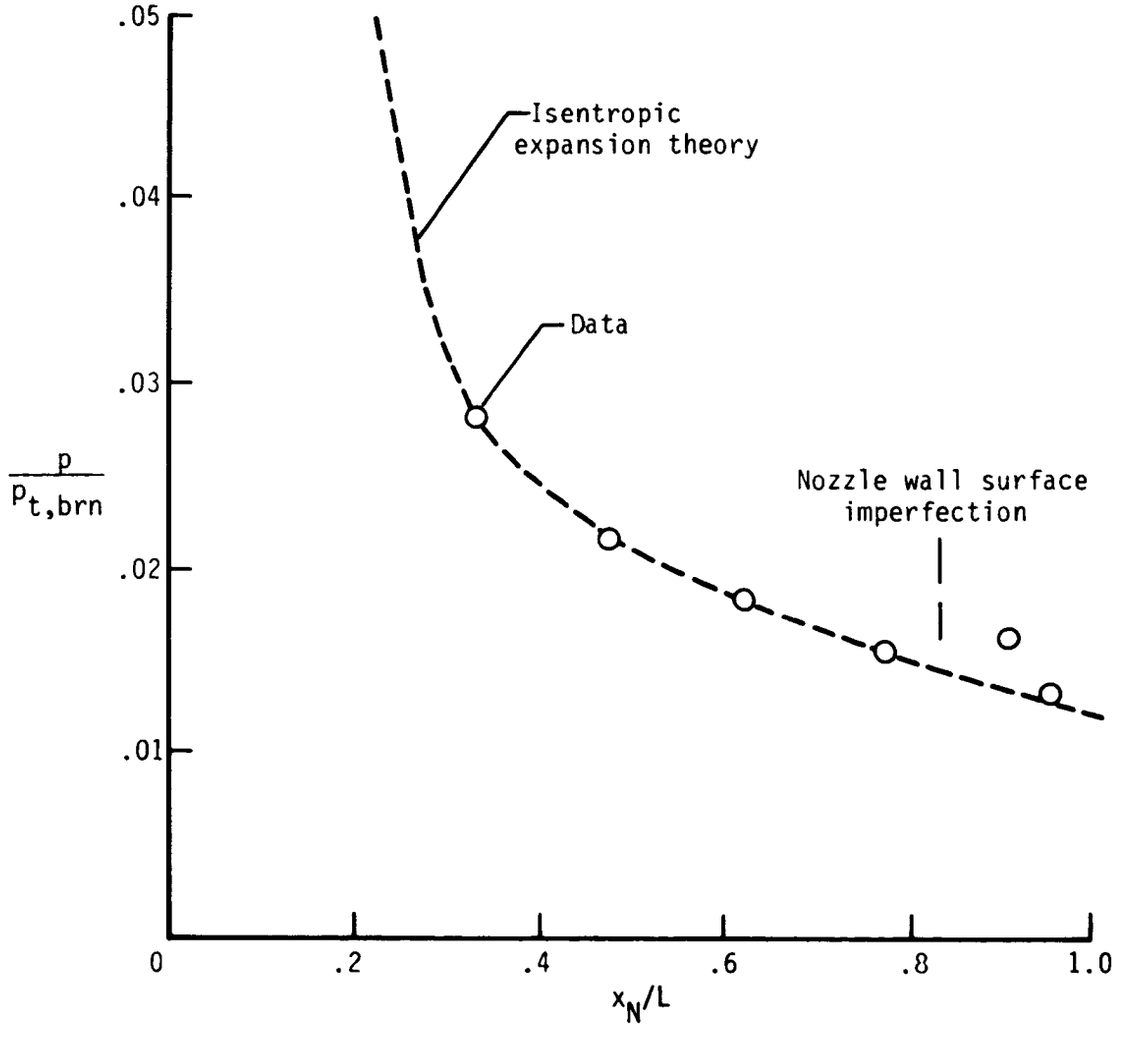

Figure 23. Langley Mach 4 Scramjet Test Facility nozzle wall pressure distribution. $P_{t,\mathrm{brn}} = 92$ psia; $T_{t,\mathrm{brn}} = 1630°\mathrm{R}$; $M_{\mathrm{noz}} = 3.5$; and $L = 50.845$ in.

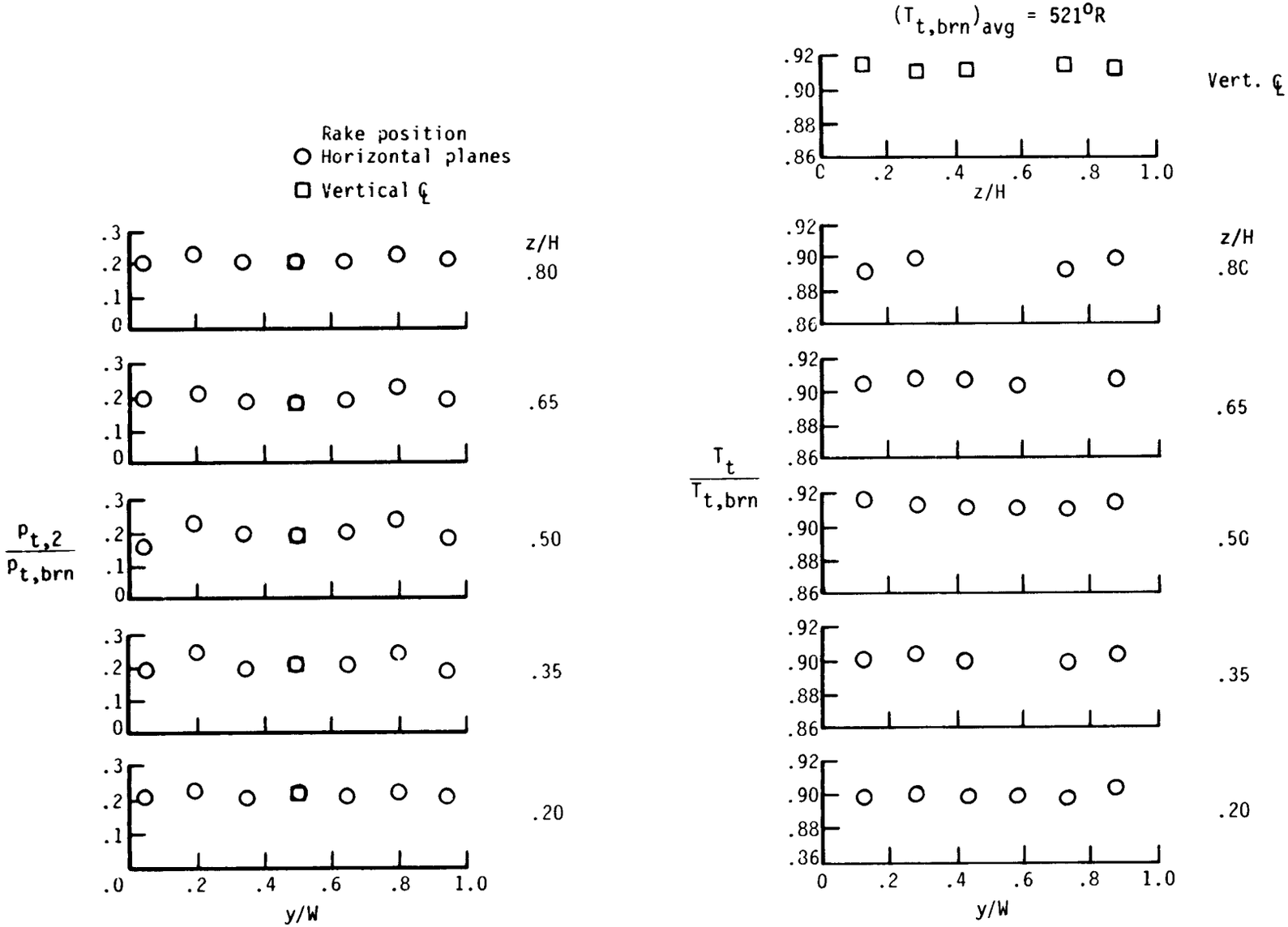

(a) Pitot-pressure profiles.

(b) Total-temperature profiles.

Figure 24. Mach 3.5 nozzle-exit survey results. $T_{t,\mathrm{brn}} = 520°\mathrm{R}$; $p_{t,\mathrm{brn}} = 92$ psia.

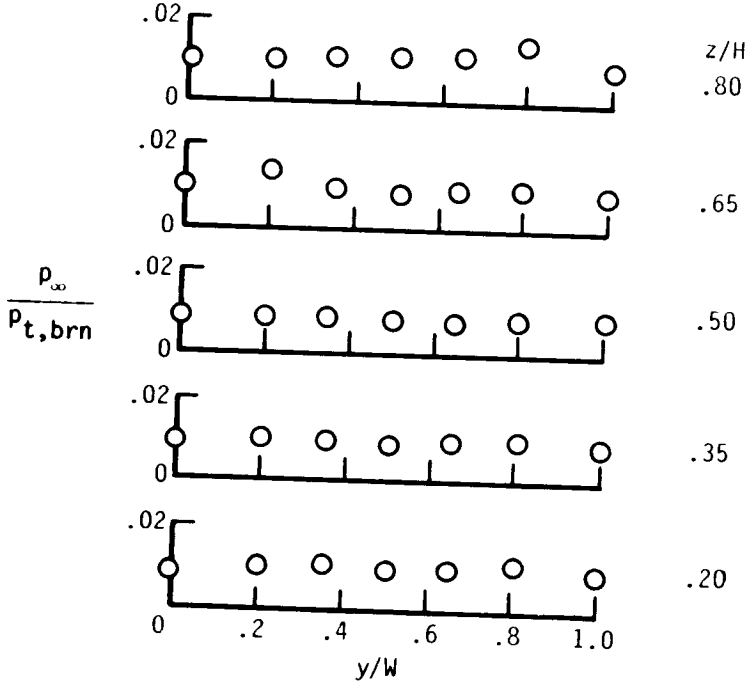

(c) Static-pressure profiles.

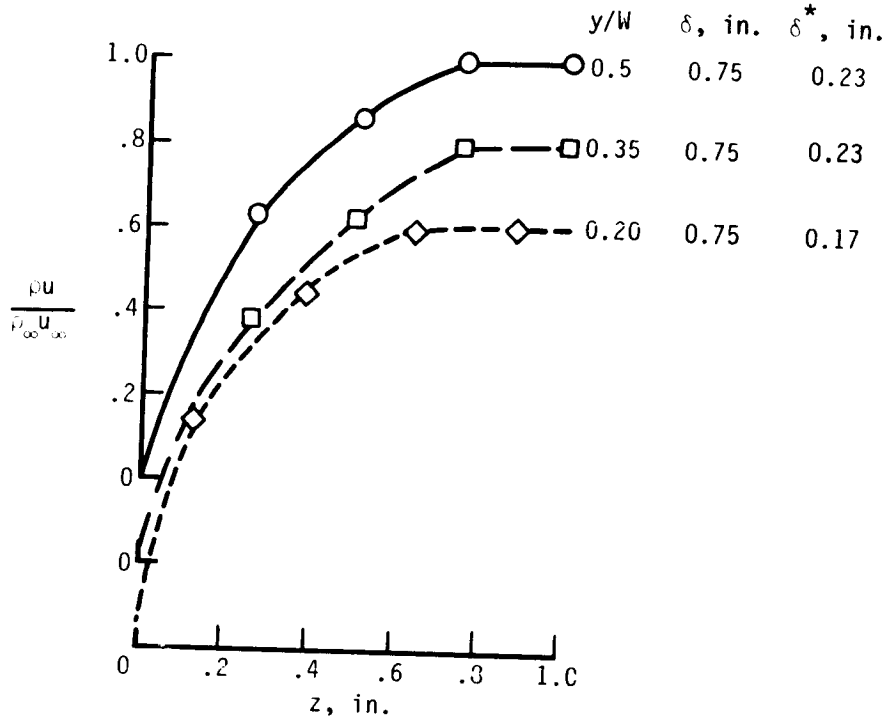

(d) Boundary-layer profiles.

Figure 24. Continued.

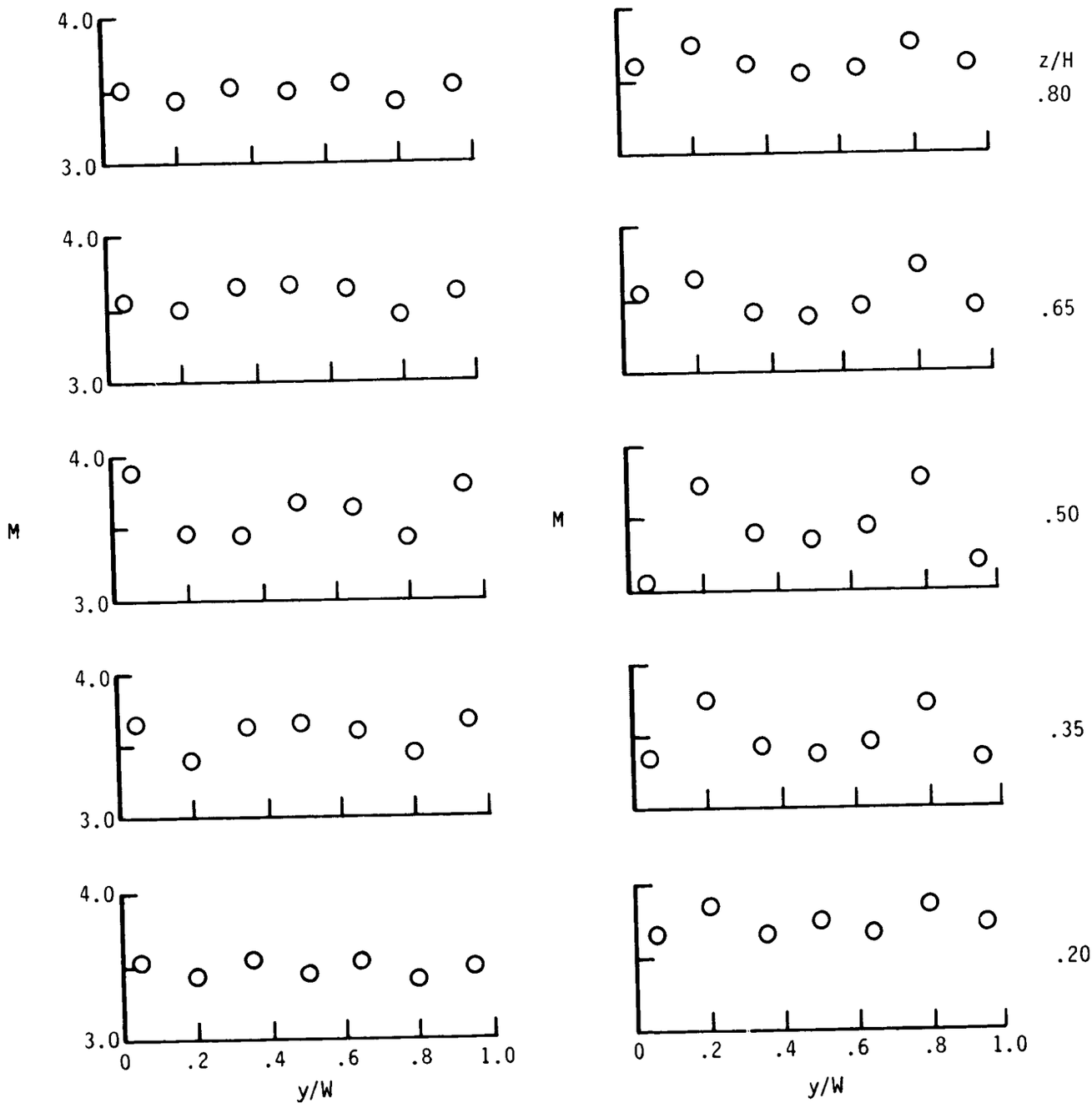

(e) Mach number profiles based on $p_{t,2}/p_{t,\mathrm{brn}}$.

(f) Mach number profiles based on $p_{\mathrm{noz}}/p_{t,2}$.

Figure 24. Concluded.

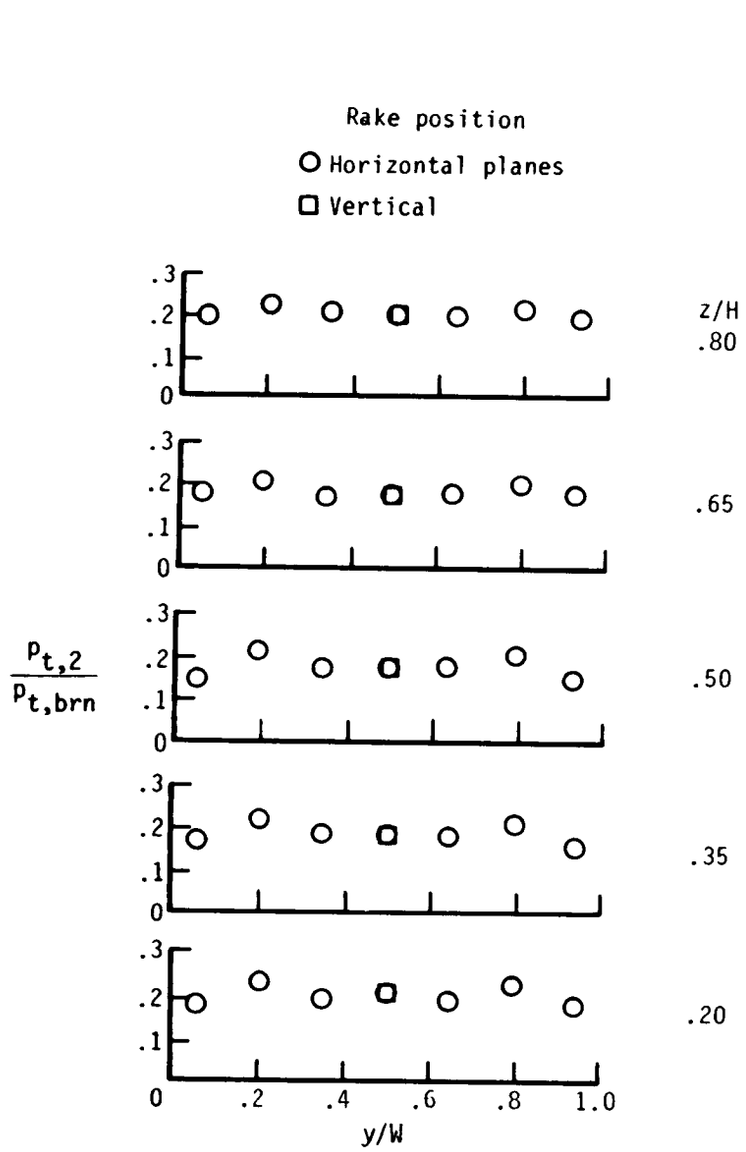

(a) Pitot-pressure profiles.

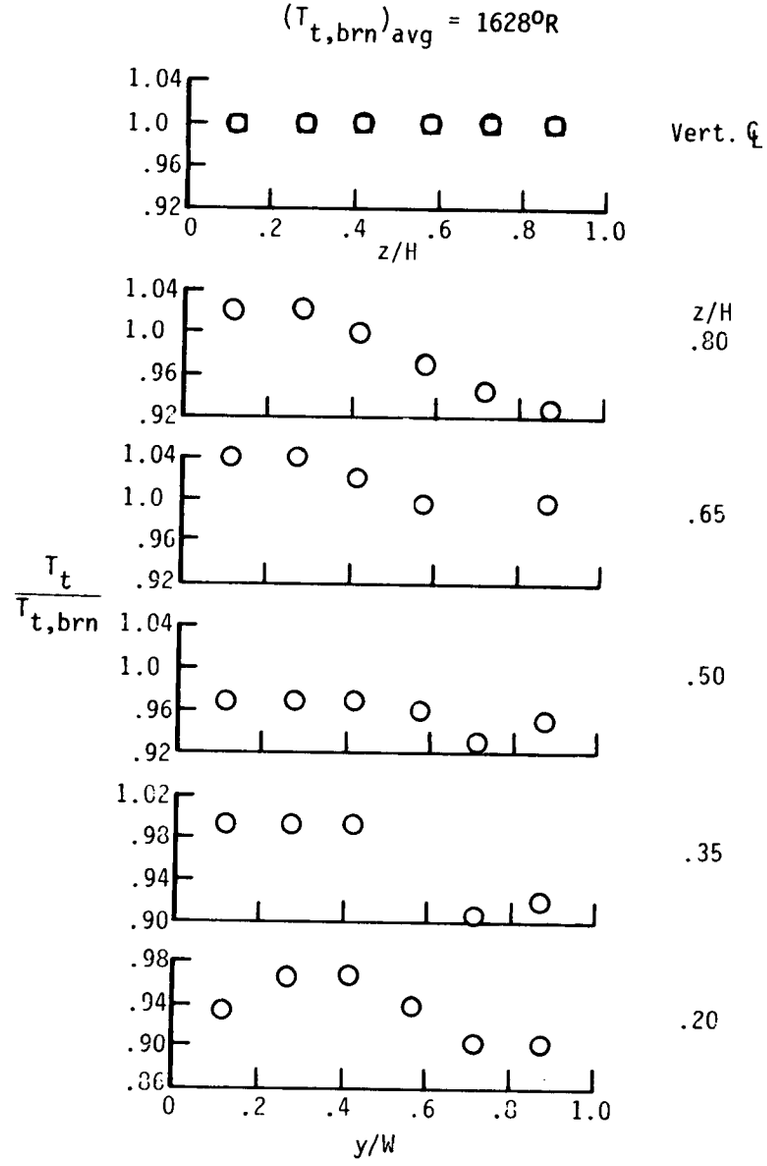

(b) Total-temperature profiles.

Figure 25. Mach 3.5 nozzle-exit survey results. $T_{t,\mathrm{brn}} = 1630°\mathrm{R}$; $p_{t,\mathrm{brn}} = 92$ psia.

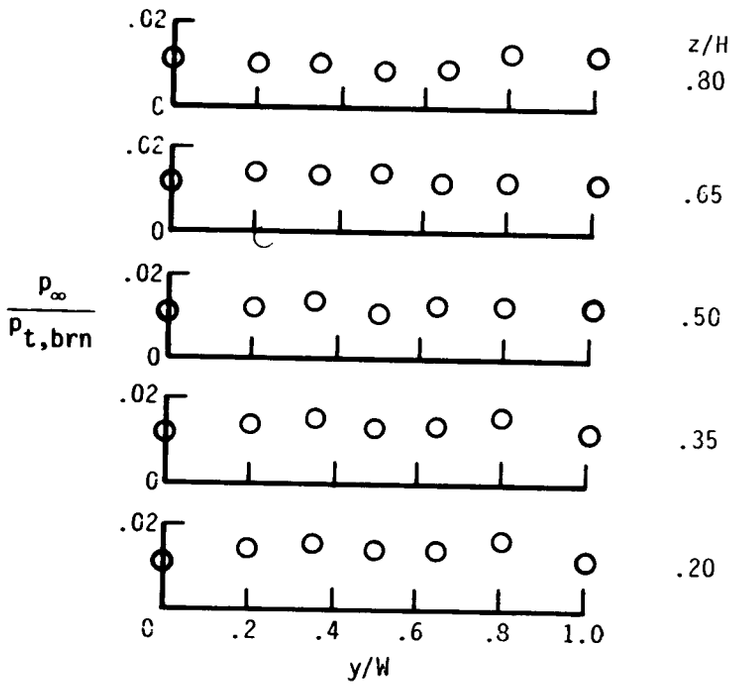

(c) Static-pressure profiles.

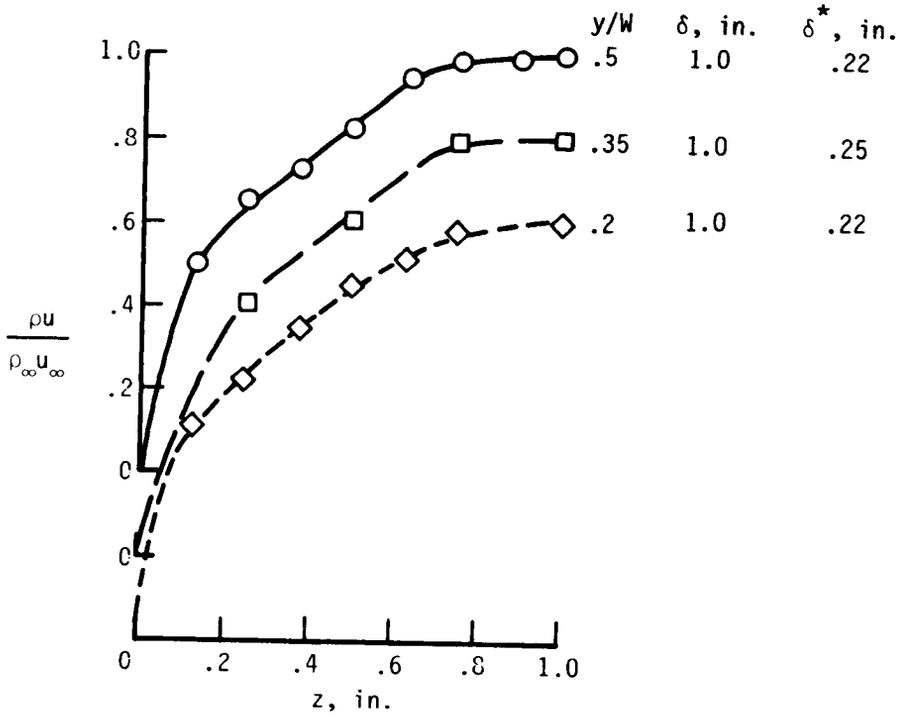

(d) Boundary-layer profiles.

Figure 25. Continued.

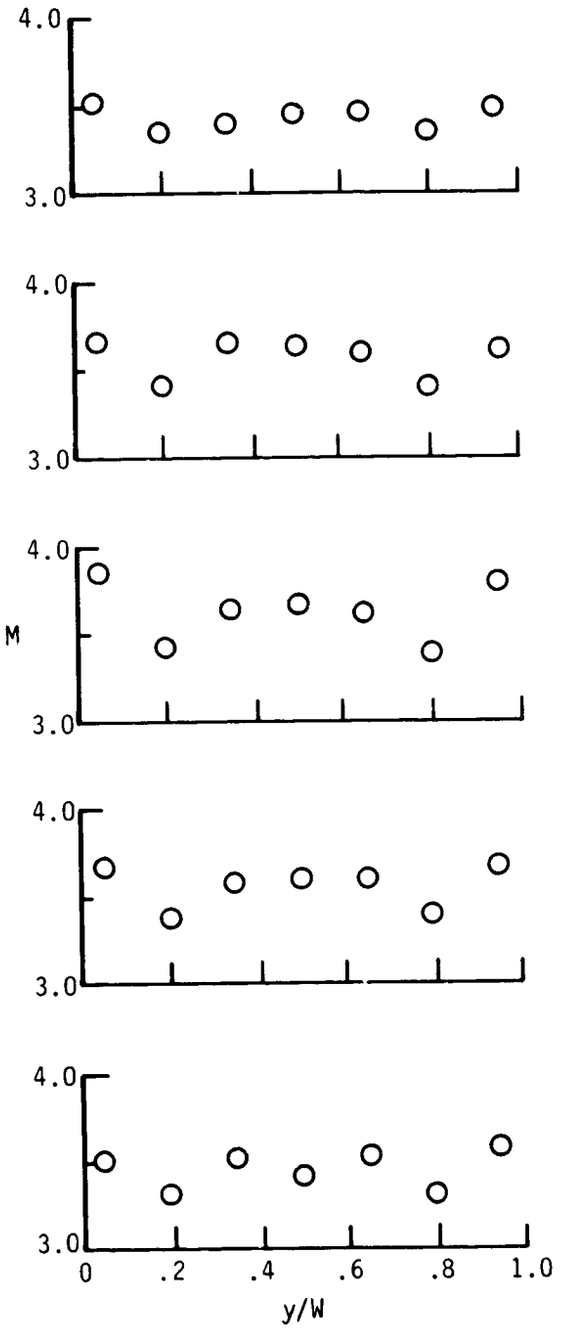

(e) Mach number profiles based on $p_{t,2}/p_{t,\mathrm{brn}}$.

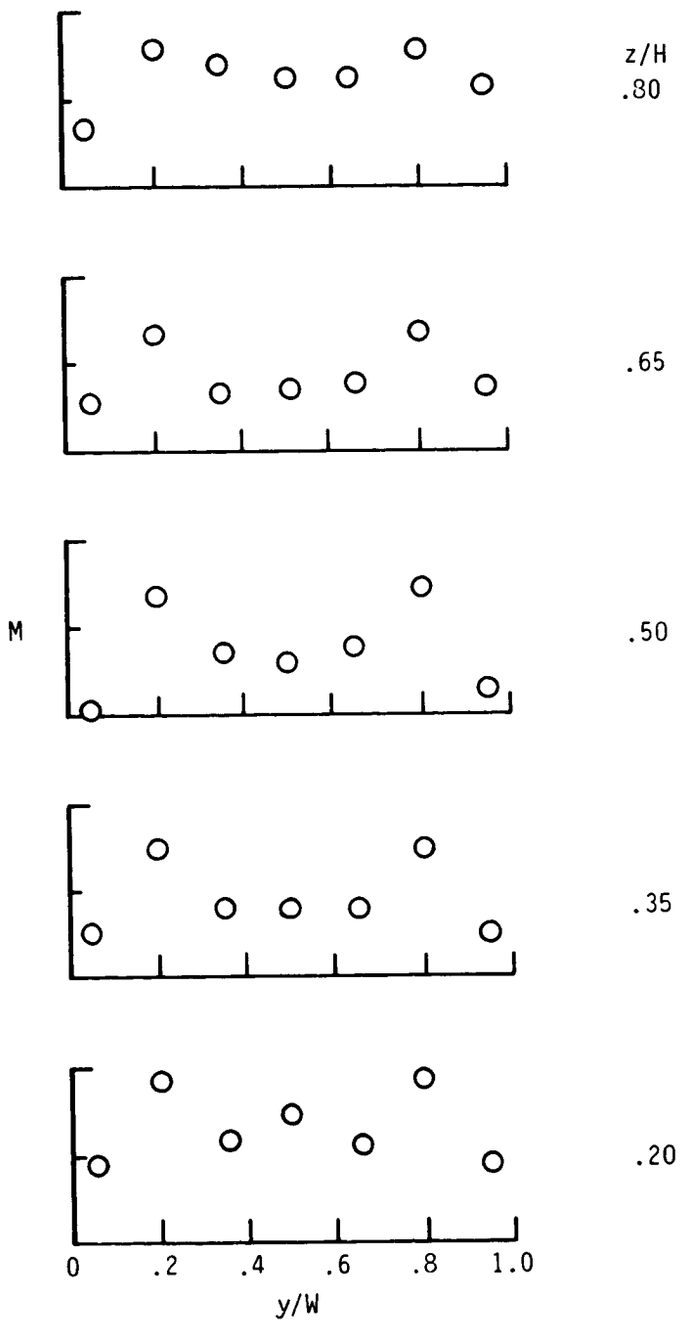

(f) Mach number profiles based on $p_{\mathrm{noz}}/p_{t,2}$.

Figure 25. Concluded.

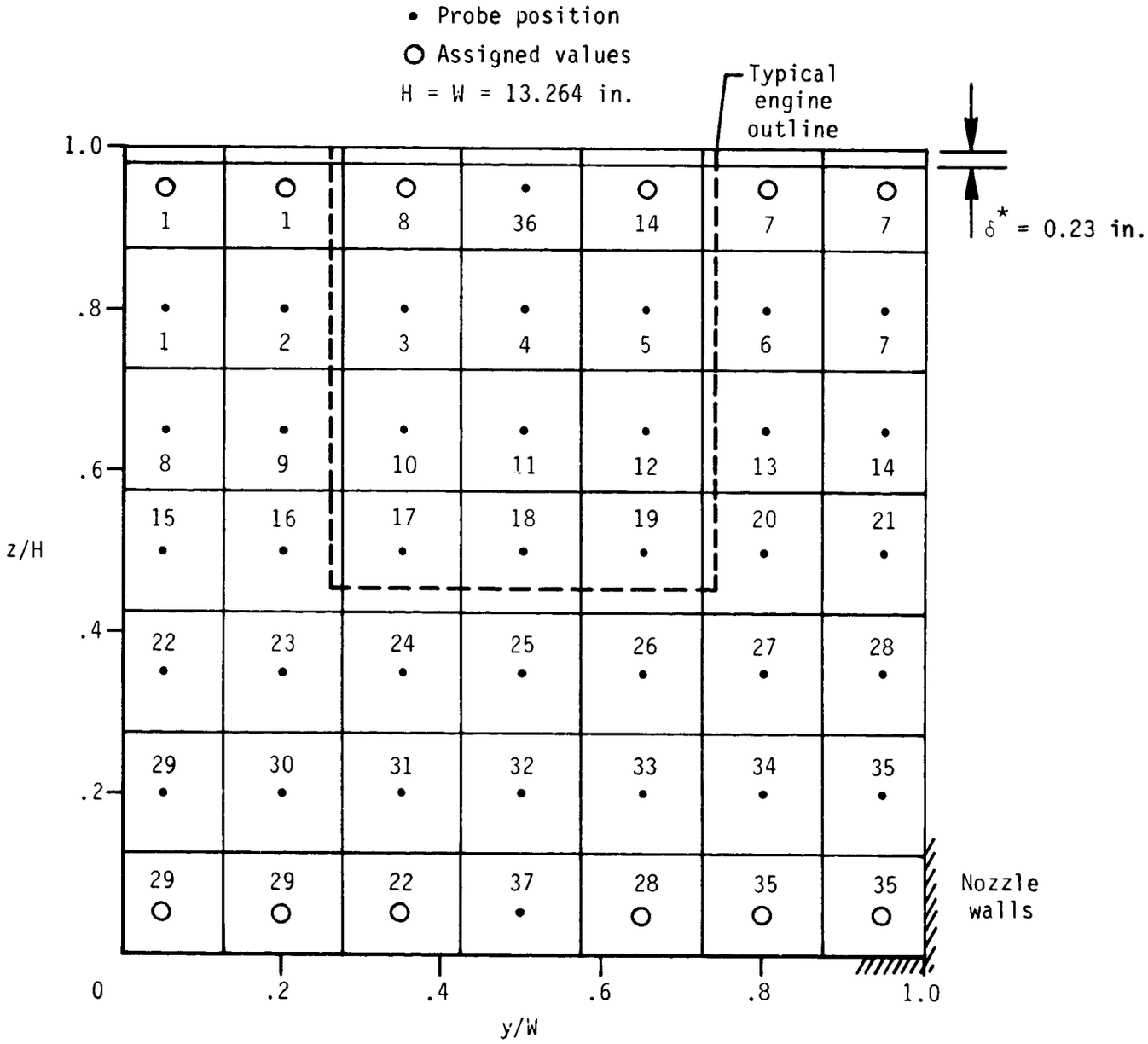

Figure 26. Area assignments for nozzle mass flow integration.

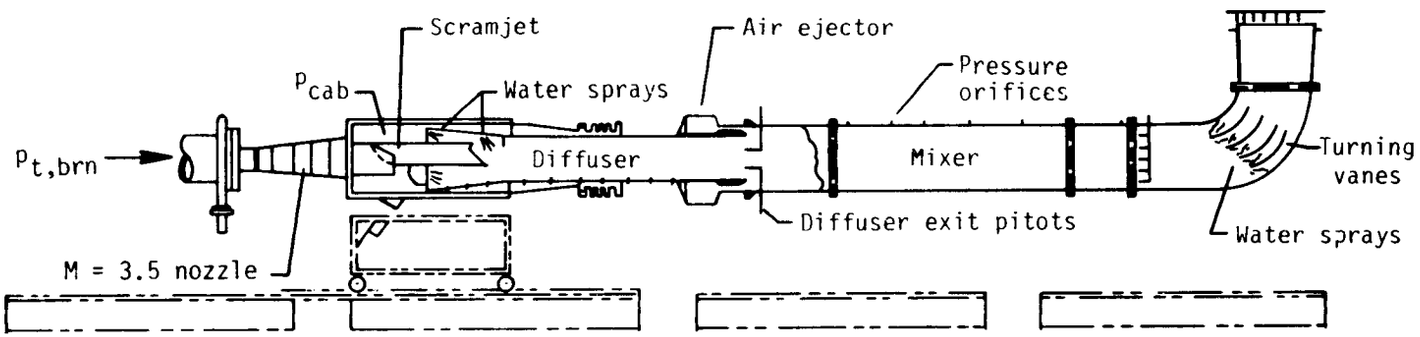

(a) Setup and measurement relative locations.

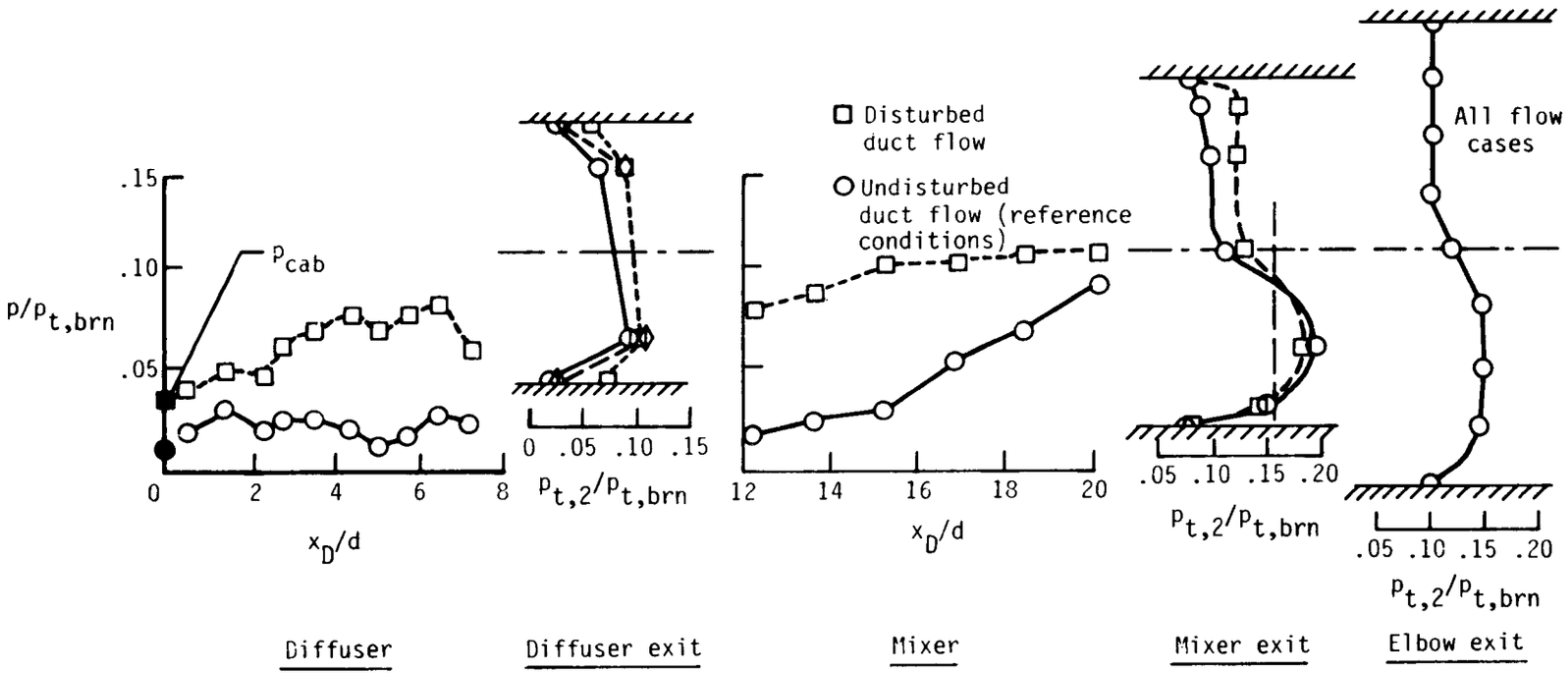

(b) Pressure measurement results.

Figure 27. Exhaust-duct flow measurements in Langley Mach 4 Scramjet Test Facility which indicated facility-engine interactions.

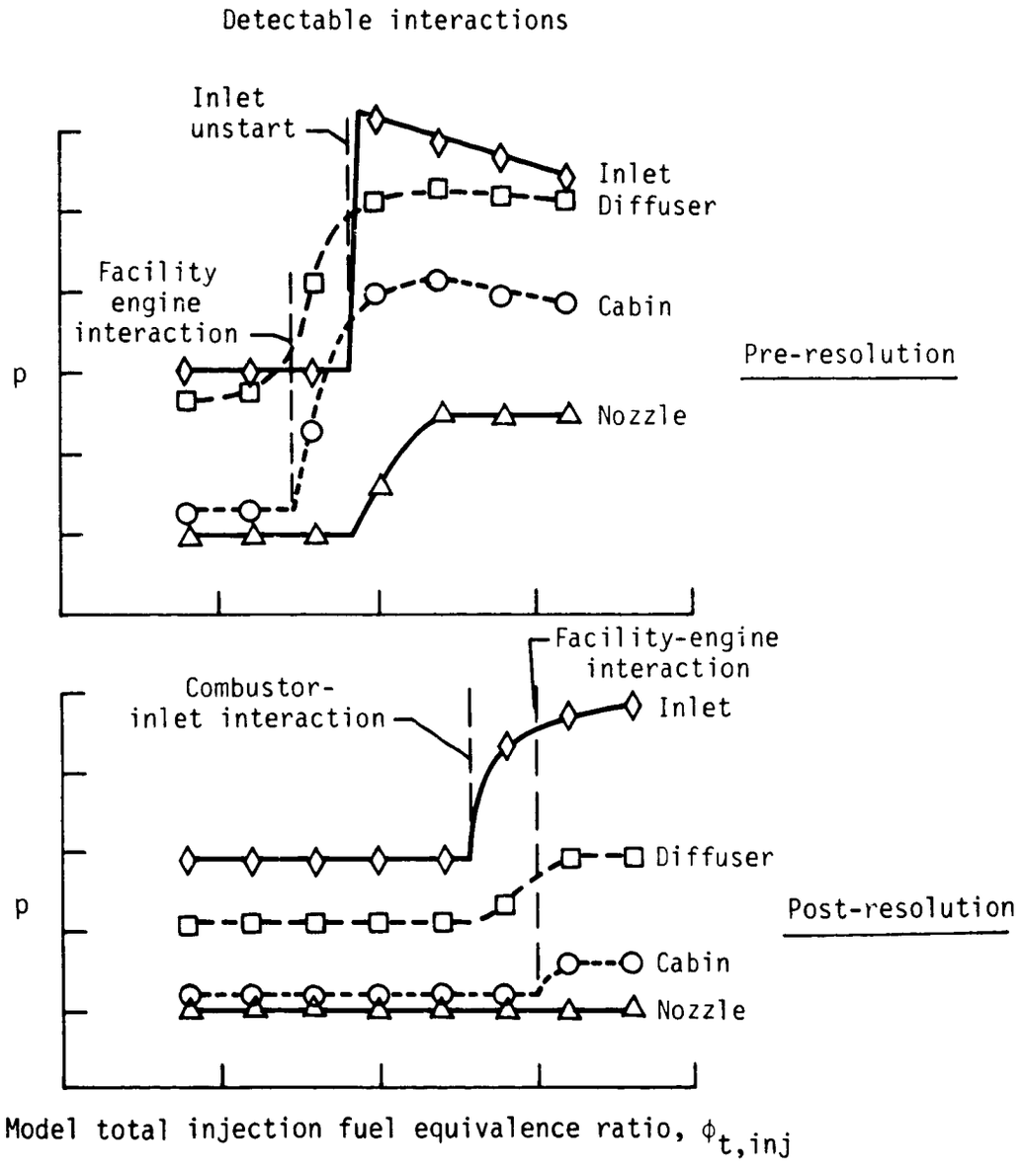

(c) Pressure measurement trends that indicate resolution of interaction problem.

Figure 27. Concluded.